Chemistry Department, University of Fribourg

Master Thesis

SYNTHESIS AND COMPUTATIONAL STUDY OF NEW GEODESIC POLYARENES DESIGNED FOR MOLECULAR HYDROGEN STORAGE AND INVESTIGATION OF THE DAKIN-WEST REACTION MECHANISM

Nathalie Joset

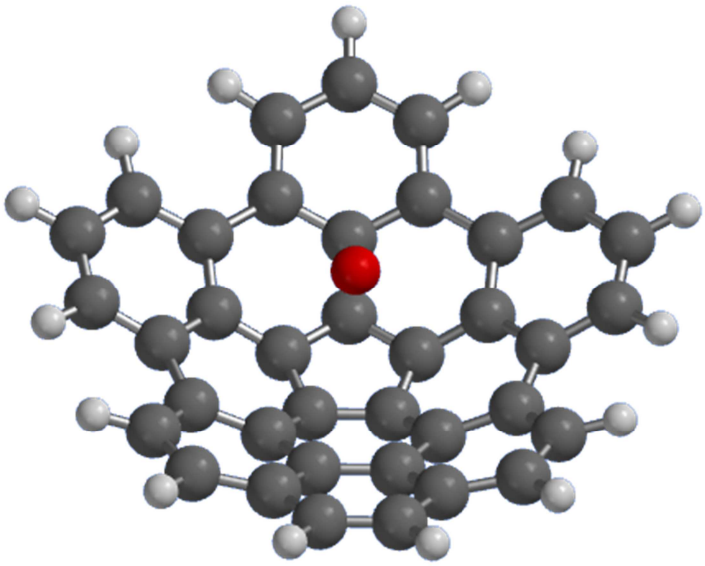

Supervisor

Prof. Dr. Titus A. Jenny

Fribourg, June 2013

Abstract

This work presents the synthesis of a new geodesic polyarene molecule based on corannulene's motive and especially designed for hydrogen storage. Indeed such curved systems are bearing a dipole moment which can polarize H_2 molecules resulting in their adsorption. The complexation of our target molecules with alkali ions would increase their dipole moment as well as the interstitial volume between the molecular stacks thus increasing the hydrogen storage capabilities.

In the first part, DFT calculations were undertaken to compare our target molecule with other curved systems and to point out the advantages or inconvenients for hydrogen storage applications.

Two main synthetic pathways were postulated, the first one starting from 2,6-difluoroacetic acid and the other starting from 2,6-dichlorophenylacetic acid. In the first it was planned that the cyclized target molecule would be obtained by fluorhydric acid elimination which was a recently discovered means of curvature introduction; the second would result of flash vacuum pyrolysis or palladium catalyzed reaction which are already well known for such purposes.

Unfortunately problems were encountered at the first step in each pathway, namely during the bisbenzyl ketone synthesis. The Dakin-West reaction was initially explored, but it proved to be inefficient and because its mechanism was not well understood, computational calculations supported by ESI-MS measurements were undertaken. Bisbenzyl anhydride was identified as intermediate, thus it was tested as a starting reagent treated with 4-dimethylaminopyridine but without success except when starting from unsubstituted 2-phenylacetic anhydride. For each pathway Claisen condensation was tested and offered the desired bisbenzyl ketone from the corresponding ester, but only in poor yields. A third approach in which 2-(2,6-dichlorophenyl)acetyl chloride was reacted with a Grignard reagent formed from 2-(bromomethyl)-1,3-dichlorobenzene and magnesium was tested. Unfortunately Wurtz coupling between brominated species was mainly observed thus hindering the production of bisbenzyl ketone as major product.

Acknowledgments

This work was achieved in the scope of the Master thesis under the supervision of Prof. Titus A. Jenny at the Department of Chemistry, University of Fribourg (Switzerland).

I would especially thank…

… Prof. Titus Jenny for accepting me in his research group and for sharing his valuable knowledge and passion with me.

… Prof. Thomas Bally for his acceptance as expert for this Master Thesis and for the numerous advices and help during my studies.

… my family, Carole, Suzy and Laurent for their support during all my studies.

… Sofia Martin Caba for her friendship and for accepting me in her laboratory.

… every colleagues with whom I shared beautiful moments.

… Nunu for its ongoing support in everything.

Contents

Abbreviations

Cy	Cyclohexane
DCC	N,N‘-Dicyclohexylcarbodiimide
DCM	Dichloromethane
DFT	Density Functional Theory
DIPEA	N, N-diisopropylethylamine
DMAP	4-Dimethylaminopyridine
Eq	Equivalent
ESI-MS	Electospray ionization mass spectrometry
Et_3N	Triethylamine
EtOH	Ethanol
Exp.	Experimental
FVP	Flash vacuum pyrolysis
GC	Gaz chromatography
HOMO	Highest occupied molecular orbital
IR	Infra-red
LDA	Lithium diisopropylamine
LUMO	Lowest unoccupied molecular orbital
MeCN	Acetonitrile
MIM	1-Methylimidazole
MS	Mass spectrometry
MWNT	Multiwalled nanotube
NMR	Nuclear magnetic resonance
PAH	Polyaromatic hydrocarbon
PEM	Polymer electrolyte membrane *or* Proton exchange membrane
Ppm	Part per million
R.t.	Room temperature

Rxn	Reaction
Sat.	Saturated
THF	Tetrahydrofurane
UPLC	Ultra-high Pressure Liquid Chromatography
Wt	Weight

1 INTRODUCTION

1.1 Hydrogen fuel cells

Many efforts to reduce greenhouse gas emissions and the dependence on finite non-renewable fuel resources have led to the development of a variety of alternative energy solutions. Of specific interest is the hydrogen fuel cell, which converts the chemical energy of hydrogen into electricity through chemical reaction with oxygen. Such devices are different from traditional batteries in that they require a constant source of hydrogen and oxygen to run, but an advantage is their continual electricity production as long as these inputs are supplied. There are many types of fuel cells, mainly differing by the electrolyte they use. Hereafter is represented a schematic diagram of cell configuration of a polymer electrolyte membrane (PEM) fuel cell also known as proton exchange membrane fuel cell (*Figure 1*). [1]

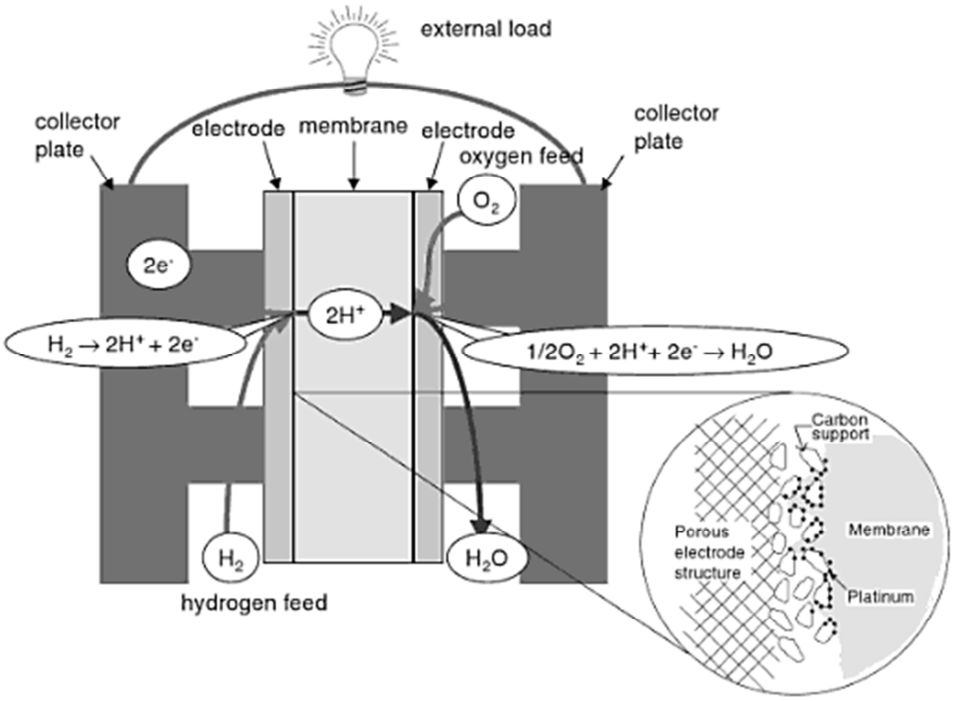

***Figure 1**: Basis principle of operation of a PEM fuel cell*

At the heart of a PEM fuel cell is a polymer membrane that acts as electrolyte which is impermeable to gases but which conducts protons (hence the name proton exchange membrane). The membrane is squeezed between the two porous electrodes typically made of carbon. At the interface between the porous electrode and the polymer membrane is a layer of catalysts particles, typically platinum supported on carbon where electrochemical reactions occur. Molecular hydrogen feeding the anode side is oxydized producing protons and electrons. The protons travel through the membrane, whereas the electrons are driven through an external circuit producing direct current electricity. Electrons come back at the cathode side where they meet the protons that went through the membrane and oxygen that

is fed on the cathode where reduction occurs. Water is created in the electrochemical reaction and then pushed out of the cell with excess flow of oxygen. This reaction in a single fuel cell produces only about 0.7 V. [2] To get this voltage up to a reasonable level, many separate fuel cells must be combined to form a fuel-cell stack. If the fuel cell is powered with pure hydrogen, it has the potential to be up to 80 % efficient. However, we still need to convert this electrical energy into mechanical work by means of an electric motor and inverter. The efficiency of this motor/inverter is about 80 %, giving an overall efficiency of about 64 %.[2]

Applications of fuel cells can be categorized in two main applications: stationary and transportation. Stationary fuel cells can be used for backup power in commercial, industrial or residential builings where they are mostly used combining heat produced by fuel cells and power production. Transportation fuel cells can be used for vehicles, including automobiles, buses, forklifts, airplanes, boats, and submarines. The global fuel cell market which was $650 millions in 2010 will be at $1.6 billion in the year 2016 promising a beautiful future. [3]

1.2 Hydrogen storage

Although stationary applications are already commercialized since 2008, the market of transportation fuel cells is less developed, especially due to difficulties in hydrogen storage, including cost, reversibility and the storage mass and volumetric densities. [4] Indeed, liquid hydrogen has a very high energy content by weight (142 MJ/kg) compared to gasoline (47 MJ/kg) [5], but a very low energy content by volume (10 MJ/L) compared to gasoline (35 MJ/L) [6]. This makes hydrogen storage particulary difficult due to the size and weight constraints of a vehicle. The following sections introduce four major technologies being currently used or actively studied for hydrogen storage.

Compressed gas

A light-duty fuel cell vehicle will carry approximately 4-10 kg of hydrogen on board to allow a driving range of more than 300 miles, which is generally regarded as the minimum for widespread public acceptance. [7] To satisfy such conditions, traditional compressed hydrogen gaz tanks would require more space than the trunk of typical automobile. Moreover, even if recent developments proved that fibre-reinforced resin can sustain pressures up to 700 bar, high pressure hydrogen storage is not a suitable storage means due to safety concerns and poor volumetric densities. [8]

Liquefaction

Liquefied hydrogen is denser than gaseous hydrogen and thus contains more energy for a given volume; by this means, it can be stored on board the vehicle, as has been demonstrated by BMW with their production-ready Hydrogen 7 vehicle collection. [9] But the major drawback is that cryogenic methods require the input of relatively large amounts of energy for maintaining a liquid at 20 K for long periods. Moreover, there is inevitably a boil-off rate which is currently in the range of l%/day. [7]

Tank insulation is required to decrease hydrogen loss but this would add weight, volume and cost of such a dispositive, restricting its range of applications.

Solid-state hydride storage

Solid-state hydride storage in which hydrogen is chemisorbed *via* chemical bonds, offers several benefits over previously presented techniques. They operate at low pressure as compared to compressed hydrogen, and don't need to be kept at cryogenic temperatures as required for liquid hydrogen storage. Hereafter several different hydrogen storage means are compared according to their volumetric hydrogen densities (*Figure 2).* [10]

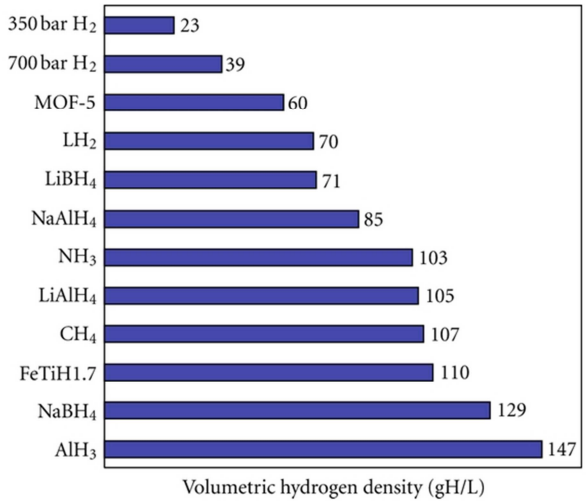

Figure 2*: Volumetric hydrogen density (gH/L) of different hydrogen storage methods including compressed gas, physisorption in a metal organic framework (MOF), liquid hydrogen (LH_2), ammonia, methane and a variety of metal and complex hydrides. These values are only for the storage medium and do not take into acoount the full system volume (e. g., tank and fuel cell)*

In the following sections, three main metal hydride classes were summarized taken from a review about metastable metal hydrides for hydrogen storage written by Graetz et al. [10]

Metal hydrides and complex hydrides

Complex metal hydrides which store atomic hydrogen through a chemical bond are often categorized by their reversibility or their ability to be rehydrogenated under moderate temperature and pressure conditions. One representative of this class is sodium aluminium hydride ($NaAlH_4$) which can release 4 wt % of hydrogen at temperatures around 160°C during catalyzed (typically 2-4 mol% Ti) thermal decomposition, thus approaching the U.S. Department of Energy (U.S. DOE) targets of 6.5 % gravimetric hydrogen density and 62 kg/m^3 volume at ambient temperature. Most importantly, the dehydrogenated material (NaH + Al) can be rehydrogenated under moderate conditions; but systems based on this kind of material (Na_2LiAlH_6, $KAlH_4$, K_3AlH_6, etc.) have an inherent heat problem posing significant engineering challenges for onboard refueling. Indeed, a large hydrogenation enthalpy

(typically greater than 33 kJ/mol H_2) is necessary to offset the large entropy change (110 – 130 J/Kmol H_2) during the hydrogenation process. Based on a generic reversible hydride with a slightly positive free energy (so that H_2 is released at pressures above 1 atm) and a 5 kg H_2 tank, roughly 83 MJ of heat is released during hydrogenation. The major drawback is that if the refueling process has to be done in 3 minutes (1.67 kg H_2/min), those 83 MJ of heat would need to be dissipated at a rate of 0.5 MJ per second which remains a big engineering challenge.

Chemical hydrides

Chemical hydrides offer high capacity and fast hydrogen desorption rates at low temperature. However these are not directly reversible under moderate hydrogenation conditions and typically require off-board chemical regeneration. From such typical materials ($NaBH_4$), molecular hydrogen is typically generated through a low temperature hydrolysis reaction (Eq. 1):

$$NaBH_4 + 2H_2O \rightarrow NaBO_2 + 4\,H_2 \qquad \text{(Eq. 1)}$$

In this type of system, a large amount of hydrogen can be generated at rapid rates that easily meet the U.S. DOE fuel flow rate target 0.02 $gs^{-1}kW^{-1}$ but after hydrolysis the reactants are left in deep thermodynamic minimums making the refueling process economically and energetically costly. Moreover, water should be readily available restricting the range of application to aquatic applications (submarines).

Ammonia borane (NH_3BH_3), which represents a class of compounds that can release hydrogen at fast rates through a low temperature thermolysis reaction, can store nearly 20 wt % of hydrogen! But its major drawback is that during the decomposition, NH_3 or B_2H_6 can be produced and even small amounts of such byproducts can destroy the proton exchange membrane of the fuel cell.

Metastable metal hydrides

Aluminium-based metastable hydrides, namely AlH_3, $LiAlH_4$, $Mg(AlH_4)_2$ and others, offer high capacities and low temperature hydrogen release; during decomposition, they can't form species which will damage the fuel cell membrane and additionally, those materials exhibit a low decomposition enthalpy, which reduces the heat required to release hydrogen at practical pressures.

This very promising technology is particularly suited for portable power systems, but is not ideal for automotive applications especially because of the high cost for regeneration.

Adsorption in carbon nanostructures

Carbon structures as single and multiwalled nanotubes (MWNTs) [11], nanofibers [12], activated carbon, fullerenes [13] and geodesic polyarenes (*Figure 3*) have an enormous potential in hydrogen storage technologies, especially for onboard vehicle storage.

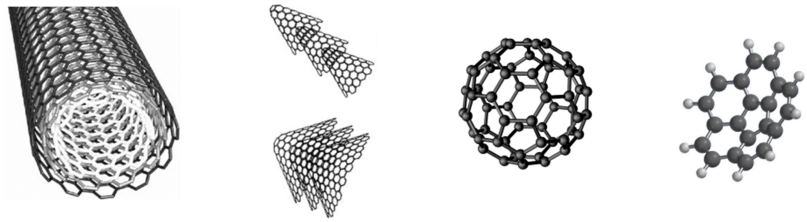

***Figure 3**: From the left MWNT, nanofibers, fullerene and corannulene*

Their major advantages are their high volumetric and gravimetric densities. However, there is a serious drawback. On the one hand, the ease of adsorbing and desorbing H_2 at ambient temperatures is limited because physisorption energies are too low (typically < 10 kJ/mol H_2). On the other hand, chemisorption energies are too high (typically > 10 kJ/mol H_2). [10] Indeed, physisorption is a process where the adsorption of hydrogen molecules is due to van der Waals attractive forces between carbon and hydrogen whereas in chemisorption, hydrogen molecules are covalently bonded to the carbon atoms. Each carbon atom in geodesic polyarenes is sp^2 hybridized and bonded with three other carbon atoms. Due to the dangling π-bond, there can be at most one hydrogen atom stored per carbon atom. The maximum storage is larger than in the physisorption process, but the major drawback is that desorption of hydrogen atoms requires higher temperature. [14] It should also be taken into account that the storage system would be capable of being recharged at the filling station in a few minutes. Thus, physisorption is thought to be the most interesting process for onboard storage.

1.3 Geodesic polyarenes

This latter class of potential hydrogen storing material and specifically geodesic polyarenes is the interest of the present work. Many kinds of bowl-shaped molecules like corannulene **1** ($C_{20}H_{10}$) pentaindecorannulene **2** ($C_{50}H_{20}$) and tetraindecorannulene **3** ($C_{44}H_{18}$) have been computationally studied [15] and show that such structures are really good candidates for hydrogen storage (*Figure 4*).

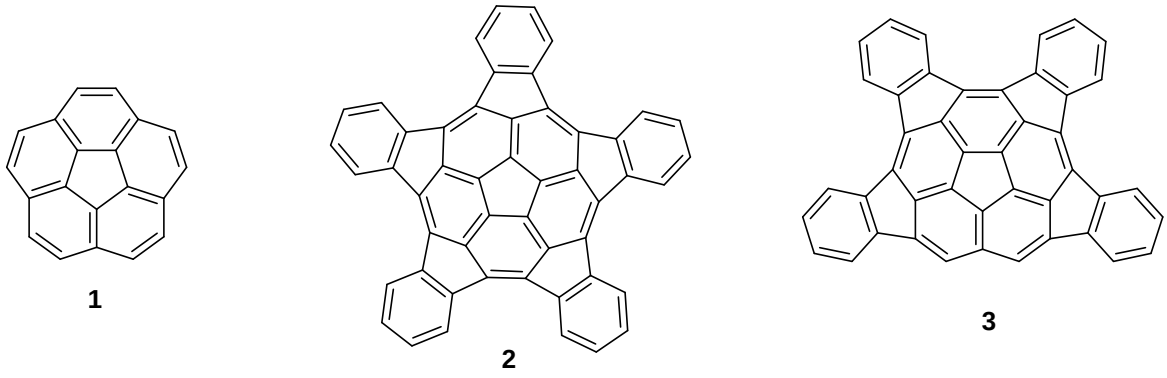

Figure 4*: Corannulene* ***1****, pentaindecorannulene* ***2*** *and tetraindecorannulene* ***3*** *structures*

Indeed, they are characterized by curved π systems composed of pyramidalized carbon atoms (*Figure 5*) [16] and one of their particularities is that they bear a permanent electrical dipole moment able to induce a dipole moment on H_2 molecules resulting in their adsorption.

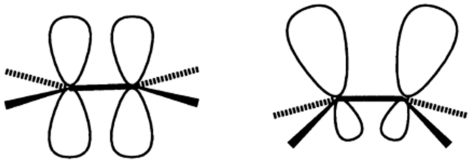

Figure 5*: Planar π system (left) and pyramidalized carbon (right)*

Hydrogen uptake of **1** was experimentally measured and found to be 1.5 wt. % at 77 K and 45 bar [17] and 0.8 % at 298 K and 72 bar. [18] These values are significantly lower than those required by the U.S. DOE, but the latter conditions should be more practicable. Using DFT calculations, Scanlon et al. first found that corannulene dimers arranged in a sandwich (local minimum) or T-shape (global minimum) geometry. They then run molecular dynamical simulations with hydrogen molecules by keeping fixed the adsorbent molecules in their initial positions. Interlayer distance (ILD) and intermolecular distance (IMD) where calculated at the B3LYP/6-311G(d,p) level (*Figure 6*). Molecular dynamics calculations showed that as the ILD increases from 4.8 to 8.0 Å, the weight percent of hydrogen uptake increases to values equal to or greater than 2 wt % of hydrogen at 300 K and at pressures of 46 to 139 bar.

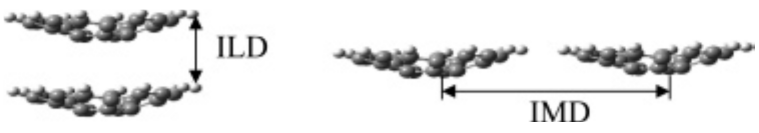

Figure 6*: Interlayer distance (ILD) and intermolecular distance (IMD) definition*

This suggests that increasing the ILD should be a solution for better hydrogen uptake. A mean of doing this is the introduction of alkali metals between corannulene units. Chen et al. have found that insertion of potassium or lithium in carbon nanotubes leads to the absorption of 14 resp. 20 wt. % of

hydrogen at 653 K and room temperatures! [19] Alkali doped corannulene monomers have been studied computationally by Banerjee et al. at the B3LYP/6-31G(d,p) level and they came to the conclusion that K^+ and Na^+ doped corannulenes can adsorb six hydrogen molecules each at the surface of the alkali. This can be attributed to the charged-induced polarization of the H_2 bond (*Figure 7*). [20]

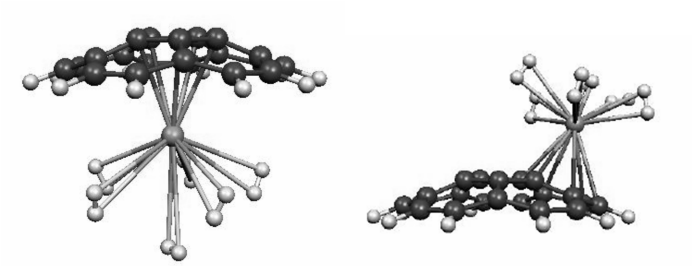

***Figure 7**: Hydrogen adsorbed on the surface of potassium (left) and sodium (right)-decorated corannulene*

A third case has been studied by Simonyan et al. by molecular simulations, namely hydrogen adsorption in charged singlewalled carbon nanotubes. They concluded that charged nanotubes lead to an increase of 10 – 20 % at room temperature in relative to the uncharged tubes adsorption. Because of the positive quadrupole moment of hydrogen, negatively charged nanotubes are preferable. [21]

Therefore the synthesis of negatively charged curved hydrocarbon systems is a valuable alternative. The mono and dianion of **1** complexed with sodium and potassium ions in the presence of [18]crown-6 ether were synthesized by Zabula and coworkers but were not tested for their hydrogen storage capabilities. [22] Crown ether additives would probably be inappropriate, increasing considerably the weight of such materials.

1.4 Brief overview of bowl-shaped molecules synthesis

Hereafter are presented synthetic methods used for curved systems preparation. Corannulene **1** was one of the first bowl-shaped molecules which has been thoroughly studied. An efficient synthetic pathway in three steps was designed by Scott et al. in 1997 with an overall yield of 20 – 25 % where ring closing of chlorinated precursor was achieved *via* flash vacuum pyrolysis (FVP) (*Scheme* 1). [23]

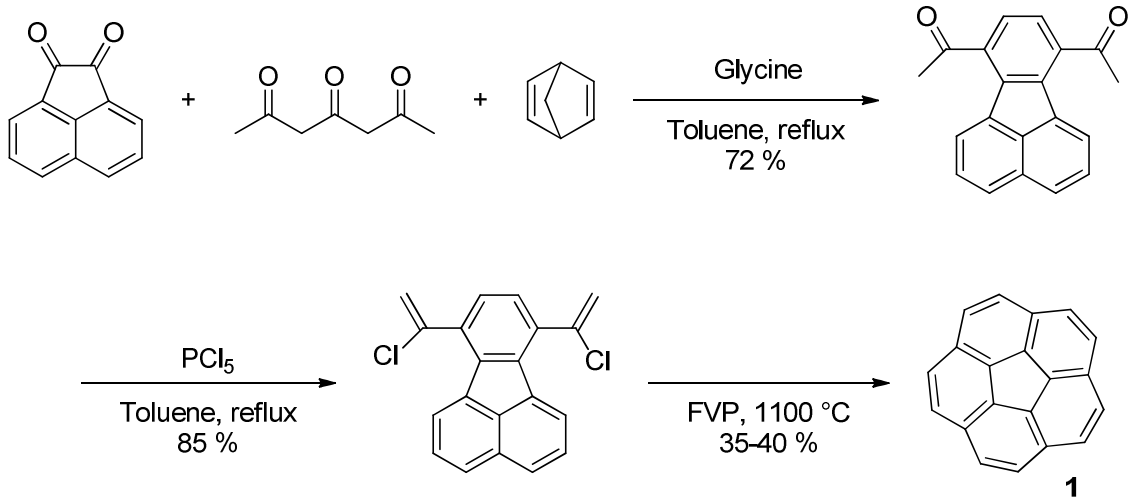

***Scheme 1**: Corannulene **1** synthesis by Scott et al. in three steps*

In 2002, they used the FVP technique to synthesize diindenochrysen **6** in 25 – 30 % overall yield starting with fluoranthene **4**. This time, the precursor for the ring closing step was brominated **5**. They found that starting with the parent hydride instead of the bromine substituted **5** dropped the yield to 0.6 % (*Scheme 2).* [24]

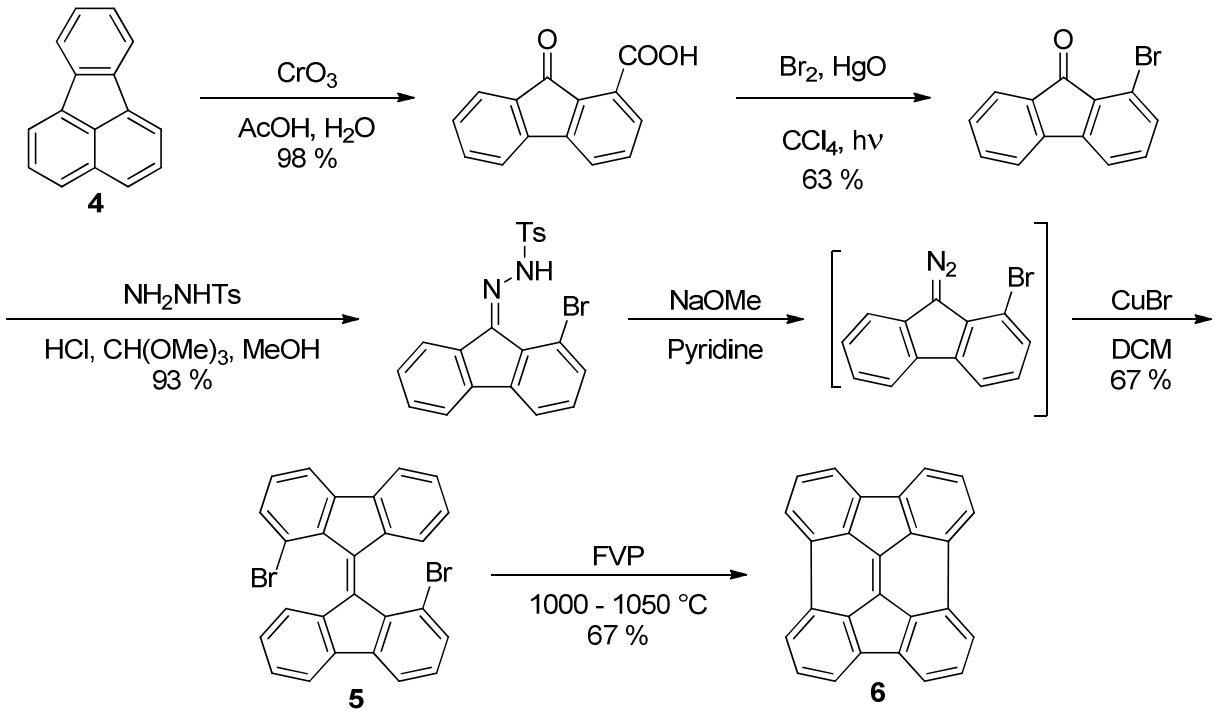

Scheme 2**: Synthesis of **6** in six steps starting from **4

Siegel et al. developed a procedure for the synthesis of **1** at kilogram scale [25] giving the opportunity of using it as starting material for the synthesis of other geodesic polyarenes. Thus, Scott L.T. et al. developed a new strategy for the synthesis of a highly curved **8** starting from **1** (*Scheme 3).* [26]

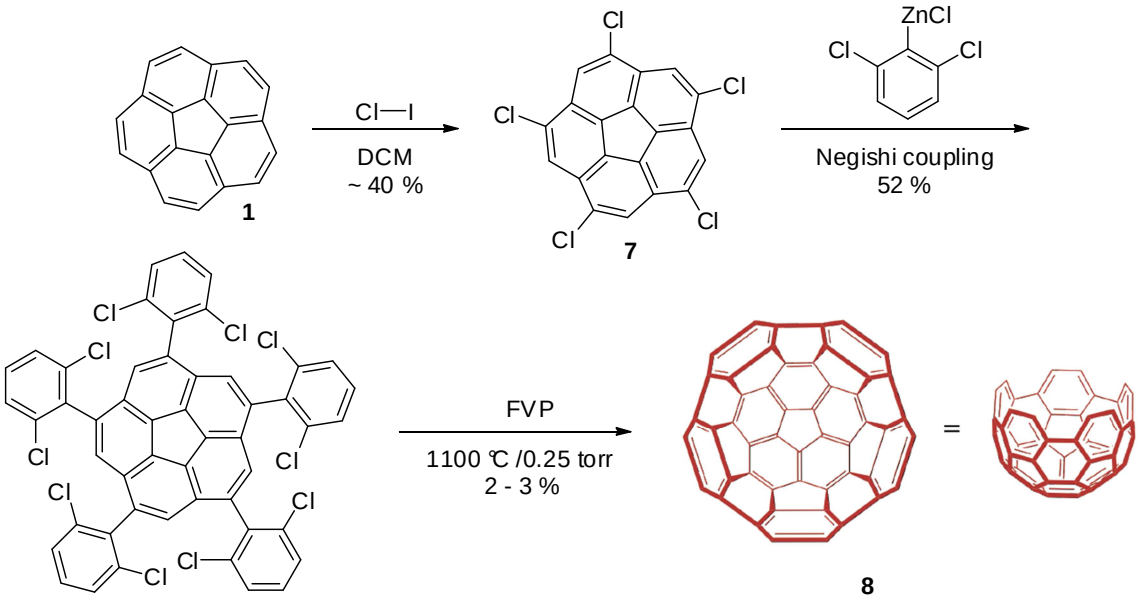

***Scheme 3**: Synthesis of $C_{50}H_{10}$ **8** using FVP for final step*

Mizyed et al. showed that the chlorination of **1** with iodine monochloride gave **7** as the major product with only a minor amount of tetrachloro derivatives. [27] Even if the last step shows only 2 – 3 % yield after chromatography, it proves that FVP is a useful tool for the introduction of curvature. Indeed, they believe that at such temperatures, the C-Cl bond rupture produces reactive aryl radicals. The high temperatures also provide the energy required to temporarily distort the intermediate species away from their equilibrium geometries, thereby bringing the transient aryl radical centers into bonding distance with otherwise remote atoms in the molecule. Thermodynamically, such reactions will be dominated by the gain in entropy resulting from the loss of 10 chlorine atoms and 10 hydrogen atoms at high temperatures. [27]

As an alternative for the harsh conditions of FVP and to get better yields, Jackson et al. reported palladium-catalyzed C-C coupling reactions for the preparation of compound **2** (*Scheme 4*) and tetraindenocorannulene **3** using microwave heating. [28]

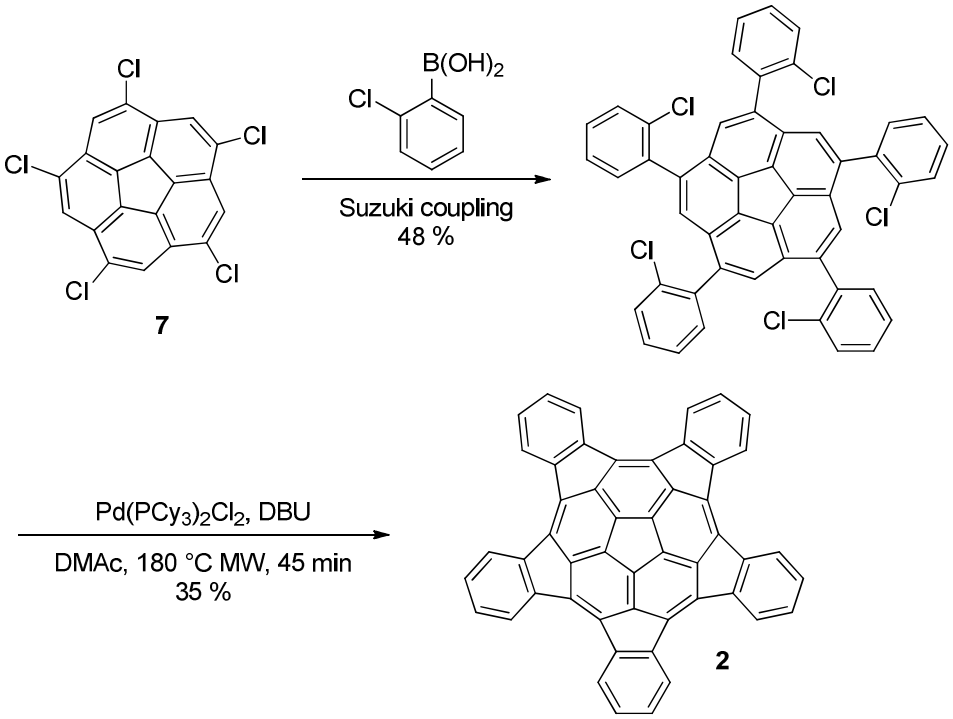

Scheme 4: *Synthesis of **2** using palladium-catalyzed ring closing method*

The procedure follows the work of Wang et al. for the synthesis of indacenopicene derivatives **9a** and **9b**. The only difference was the use of microwave instead of traditional heating. Those palladium-catalyzed reactions gave in general better yields 15 and 35 % for **2** resp. **3** and even 70 – 90 % for less curved **9a** and **9b** derivatives (*Scheme 5*). [29]

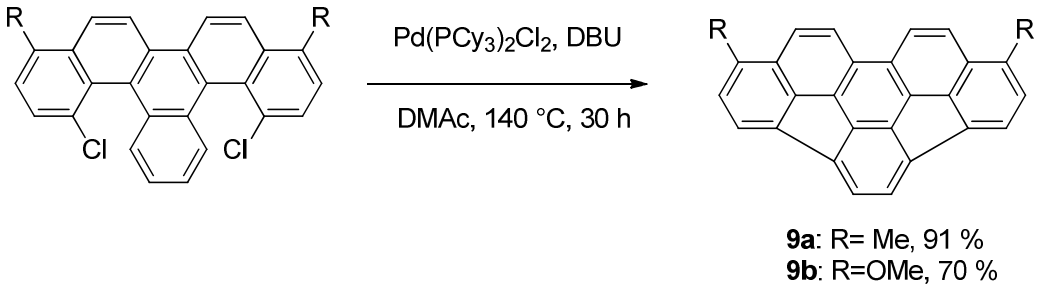

Scheme 5: *Synthesis of **9a** and **9b** using palladium-catalyzed ring closing method*

In a recent research, Amsharov and coworkers [30,31] proved that C-C bond formation would be achieved by means of HF elimination using γ-Al_2O_3 (*Figure 8*).

Figure 8: *Possible mechanism of the cove-region closure process for benzo[c]phenanthrene condensation showing coordination on the aluminium oxide surface, aromatic transition state, and Al-F bond formation*

Advantages of such an approach are the low atomic size of fluorine atoms favoring their introduction in sterically constrained cove regions and the high chemical resistance of the C-F bond which extends the scope of reactions that can be applied for precursor synthesis. [26] Moreover, the reaction conditions are really milder than those used in FVP. Indeed, γ-Al_2O_3 is activated by annealing at 500 °C for 15 min at 10^{-3} mbar pressure then mixed with the fluorinated compound and finally heated to 150 – 200 °C for achieving condensation in high yields (*Scheme 6*). These good results can be attributed to the concerted mechanism in which bond formation and rupture occur at the same time thus no reactive intermediates which might cause side reactions would be formed. The driving force of the reaction is the strong Al-F bond formation (*Figure 8*).

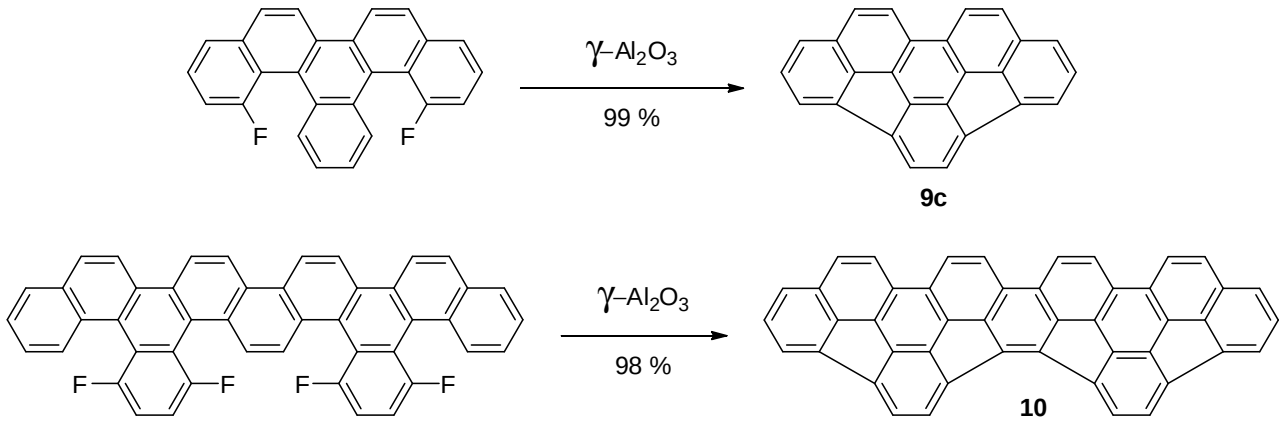

Scheme 6: *Curved* ***9c*** *and* ***10*** *syntheses by two- and fourfold ring closing via HF elimination*

However, even if fluorinated compounds seem to be good precursors for introducing curvature, their potency to prepare highly strained systems was unsuccessful so far and needs to be further explored. [32]

Nicolas Fragnière claimed having synthesized curved polyaromatic hydrocarbon **11** by achieving cyclodehydrogenation of a cyclopentadiene derivative using the Scholl reaction but only the partially oxidized bis-phenanthrene **12** was isolated (*Scheme 7*). [33]

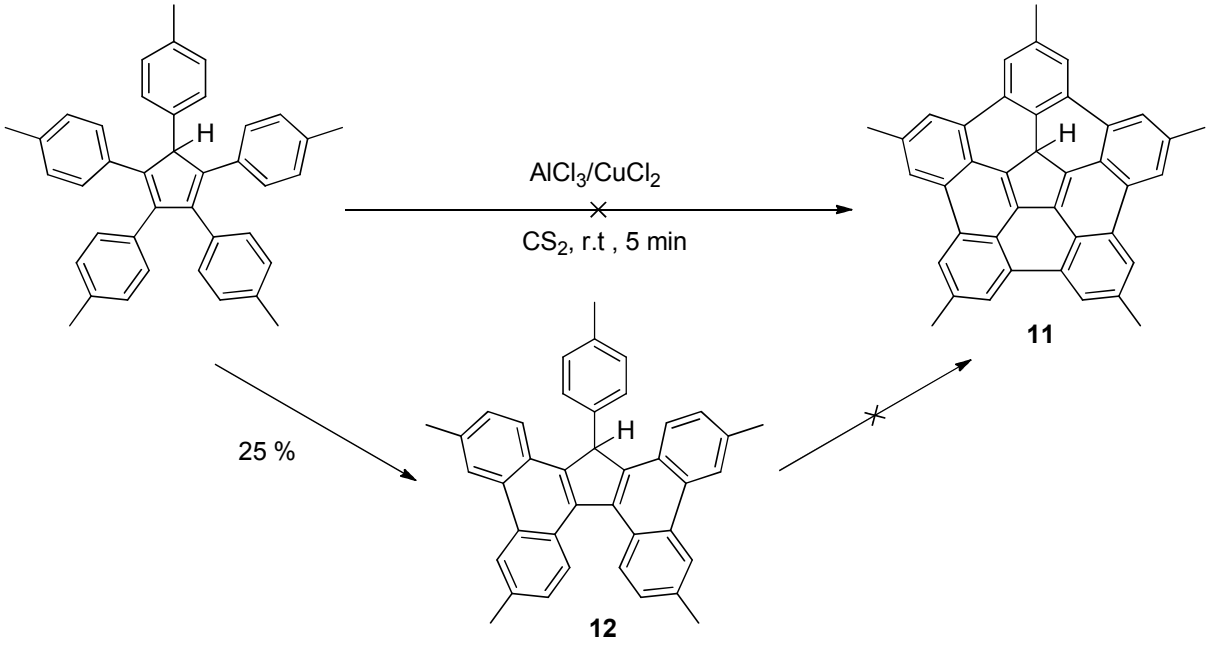

Scheme 7: *Oxidation attempts of pentaphenyl cyclopentadiene derivative to give PAH* ***11***

Starting from reagents already containing links between aromatics had been thought to favor further cyclisation. Thus, a strategy starting from pyrene quinone was developed by Pierric Weber (*Scheme 8*). [34] Unfortunately, due to rearrangements, cyclopentadiene derivative **15a** was only obtained in 18 % yield and no oxidation conditions were tested.

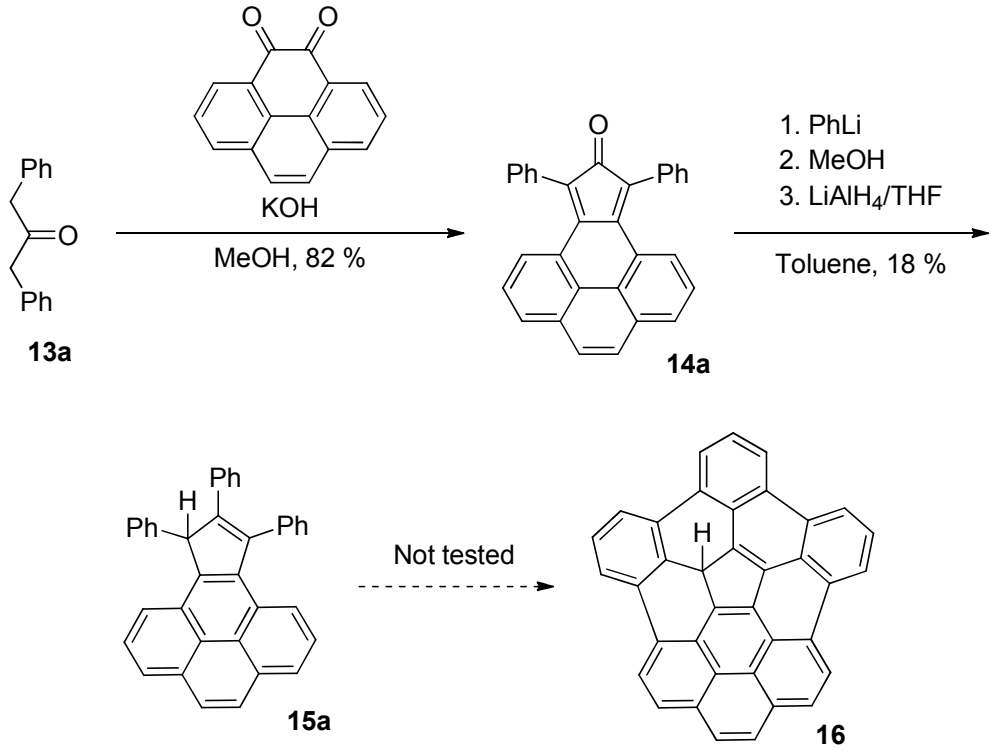

Scheme 8: *Strategy developed by Pierric Weber*

The first aim of the following work was the application of ring closure *via* HF elimination, FVP or palladium catalysis on precursors synthesized following the procedure developed by Fragnière and Weber.

1.5 Aim of the present work

In this work, new strategies were developed for the synthesis of geodesic polyarene **16** which would be a material of choice for hydrogen storage due to its increased diameter as compared to **1** (*Figure 9*). Indeed, this will rise the number of interacting sites and the interlayer distance due to the higher curvature. This diameter increase could also change a bit the curvature resulting in a probable slightly higher dipole moment value which would favor hydrogen adsorption.

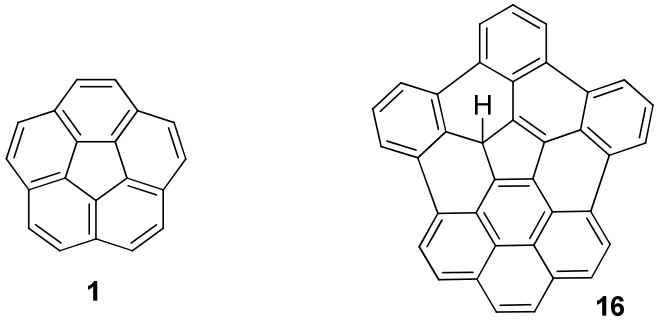

Figure 9: *Corannulene **1** and first target molecule **16***

If **16** would not show acceptable hydrogen storage capacities, it is believed that it could react with alkali hydrides (NaH *or* KH) producing alkali-curved polyarene complexes **16'K** *or* **16'Na** displaying even higher dipole moments giving rise to stronger interactions with hydrogen molecules (*Scheme 9*).

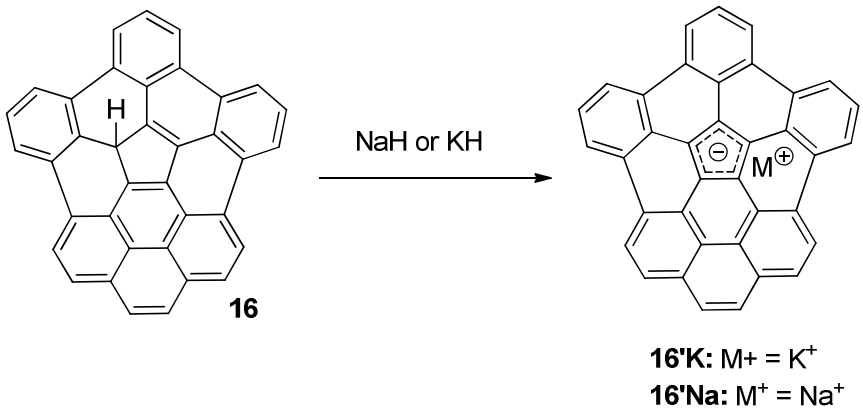

Scheme 9: *Synthesis of alkali-curved polyarene complexes **16'K** or **16'Na** through deprotonation of **16** by alkali hydrides*

Banerjee and coworkers have performed DFT calculations to find the hydrogen uptake capacity of an isolated alkali-doped corannulene molecule. They have found that hydrogen molecules bind at the surface of alkali metal preferentially. [20] This approach is interesting, albeit not really realistic, because it may be far from real solid state systems.

A more realistic aspect would be that alkali-cations could act as spacer, increasing the ILD and thus the hydrogen uptake. However, those cations would also occupy some space, thus hindering hydrogen adsorption at their location. Furthermore, it should also be kept in mind that alkali insertion will raise the weight of **16'K** and **16'Na** significantly.

Dipole moments of different curved molecules were calculated and compared with our target molecules using DFT. The distances between curved polyarenes and alkali ions were also measured to see which of **16'K** or **16'Na** will be better suited as subunit spacer.

2 RESULTS AND DISCUSSION

2.1 Computational calculations for geodesic polyarenes

In order to visualize the electrostatic potential surface and dipole moment of coronene **17**, corannulene **1**, highly curved **8**, target molecule **16** and alkali-doped complexes **16'K** and **16'Na**, computational calculations were performed in the gas phase using the hybrid exchange correlation energy functional commonly known as B3LYP [35] , implemented in the Gaussian 09 software. [36] After each geometry optimization at the B3LYP/6-311G* level, vibrational frequency calculations were achieved at the same level of theory to ensure that the molecular system was at a local minimum and to provide the thermodynamic correction factors at 298 K. Electrostatic potential surfaces were computed by running B3LYP/6-31G* single point energy calculations on Spartan '10 software [37] starting from optimized structures.

Dipole moments were obtained by single point energy calculations at the B3LYP/6-311++G(d,p) level on optimized structures. It's important to notice that it's not the purpose of the present work to accurately determine the dipolar moments; however, it's expected that it would give a qualitative comparison between the different polyaromatic hydrocarbons (PAHs).

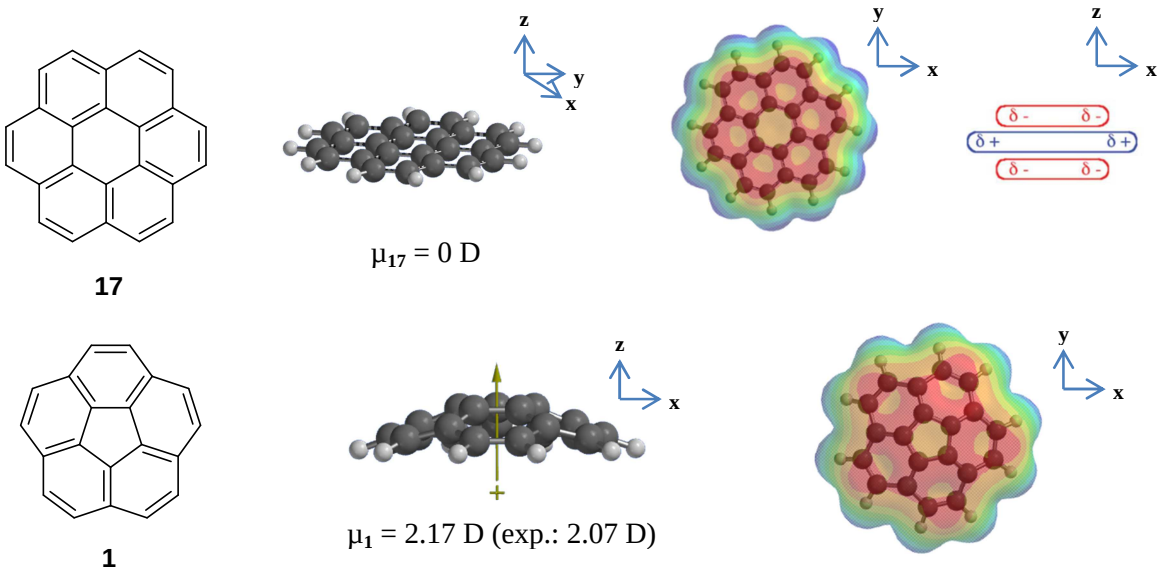

Figure 10: *Calculated dipole moments (also experimental value for **1**) and electrostatic potential surface of planar **17** and curved **1**. The regions of most negative electrostatic potential are shaded red and the most positive regions are shaded blue. Schematic qualitative quadrupole represented for coronene **17***

In *Figure 10*, two different PAHs are presented, namely coronene **17**, which is totally planar and curved corannulene **1**. Schematic illustration of the qualitative quadrupole moment of coronene is also represented. [38] In the case of **17**, all the "micro" dipoles between atoms cancel as a consequence of molecular symmetry. When curvature is introduced, the two-dimensional "micro"-dipoles still

annihilate each other but 3-dimensional ones appear. The consequence is that all the z-components are added resulting in a permanent electric dipole moment. The B3LYP method was found to be quite accurate as the difference between calculated and experimental dipole moments [18] of corannulene was only 0.1 Debye.

In *Figure 11* calculations at same level were realized for **16** and the deprotonated form **16'**. The latter allowed us to see qualitatively that concave face was more electron-rich, thus favoring the interaction with alkali cations on this side. This observation was quite surprising from a classical point of view because if electrons are only considered as negative charges, there would be a higher repulsion between them inside than outside of the bowl molecule.

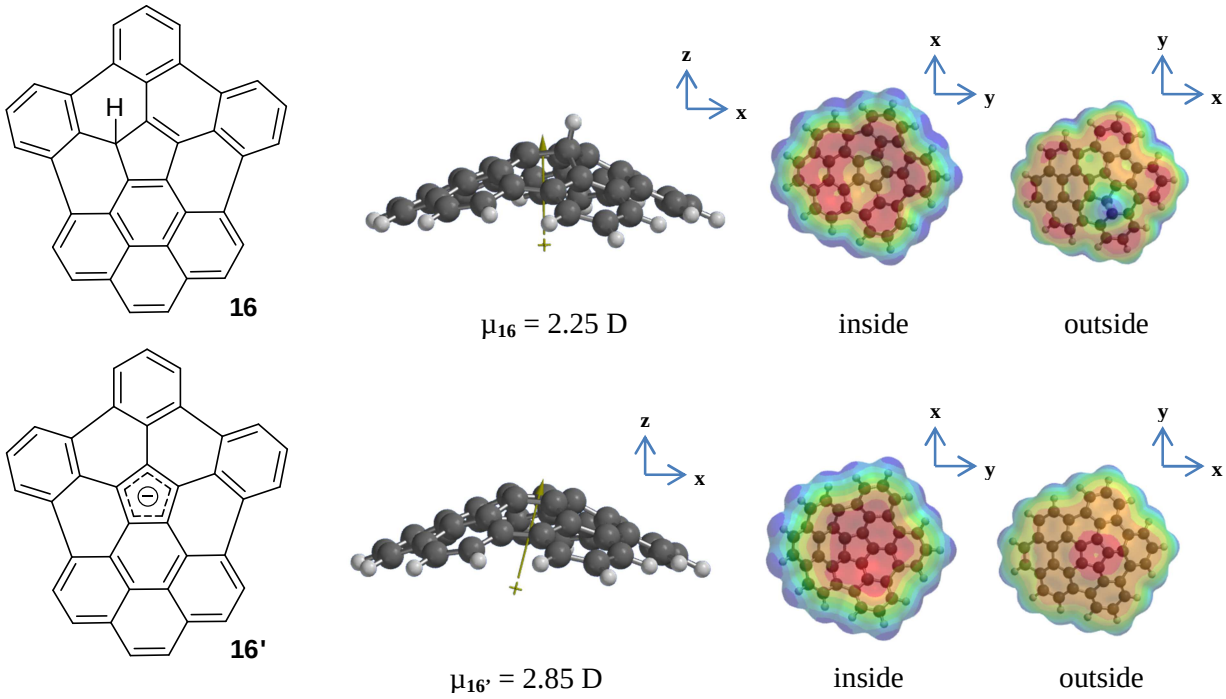

Figure 11: *Calculated dipole moments and electrostatic potential surface of* ***16*** *and its deprotonated form* ***16'***

Single point energy calculations at the B3LYP/6-311++G(d,p) level and thermal corrections from B3LYP/6-311G* frequency calculations where used to compare the energy difference between concave and convex bonding of the alkali ion in **16'K** and **16'Na** complexes. To do this, the following equations were used.

$$\Delta H_f = [E(cmpx) + H_{corr}(cmpx)] - [E(PAH) + H_{corr}(PAH) + E(ion) + H_{corr}(ion)]$$

$$\Delta S = S(cmpx) - [S(PAH) + S(ion)] \qquad (Eq.\mathbf{2})$$

$$\Delta G_f(cmpx) = \Delta H_f - T\Delta S$$

Where E(cmpx), E(PAH) and E(ion) are the total energies of complexes **16'K** or **16'Na**, polyarene **16'** and alkali ion. ΔH_f, ΔS and ΔG_f are the formation enthalpies, entropies and free Gibbs energies. Energy differences were determined by using *Eq.* ***3***.

$$\Delta G_{conv} = \Delta G_f(cc) - \Delta G_f(cx) \qquad (Eq.\mathbf{3})$$

Where ΔG_{conv} is the Gibbs free energy difference between concave, ΔG_f(cc) and convex, ΔG_f(cx) forms. For either **16'K** or **16'Na**, the concave complex was found to be favored with a ΔG_{conv} of -23.2 resp. -9.5 kJ/mol. This observation is quite different than those obtained by Banerjee et al. for corannulene alkali doped molecules. [20] Indeed, they found that the most stable sodium complex would be the convex form while those of potassium complex would adopt a concave arrangement. However they computed dipole – ion interactions of neutral corranulene with cations, while we have considered ion-ion interactions between anion **16'** and cations. Moreover, the differences between convex and concave structures are low and Mizyed et al. have elsewhere noticed that theoretical calculations give different answers for predicting which of the two π-faces is more electron rich. Indeed, they found that semi-empirical calculations give a more negative electrostatic potential on the convex surface of corannulene while higher density functional calculations predict exactly the opposite properties. Until now, no experimental tests were achieved but it's believed that better predictions are achieved by the latter DFT methods, because electron correlation is explicitly included. [27]

In *Figure 12* and *13*, properties of concave complexes **16'K** and **16'Na** and highly curved short [5,5] carbon nanotube cap **8** synthesized by Scott [26] are shown.

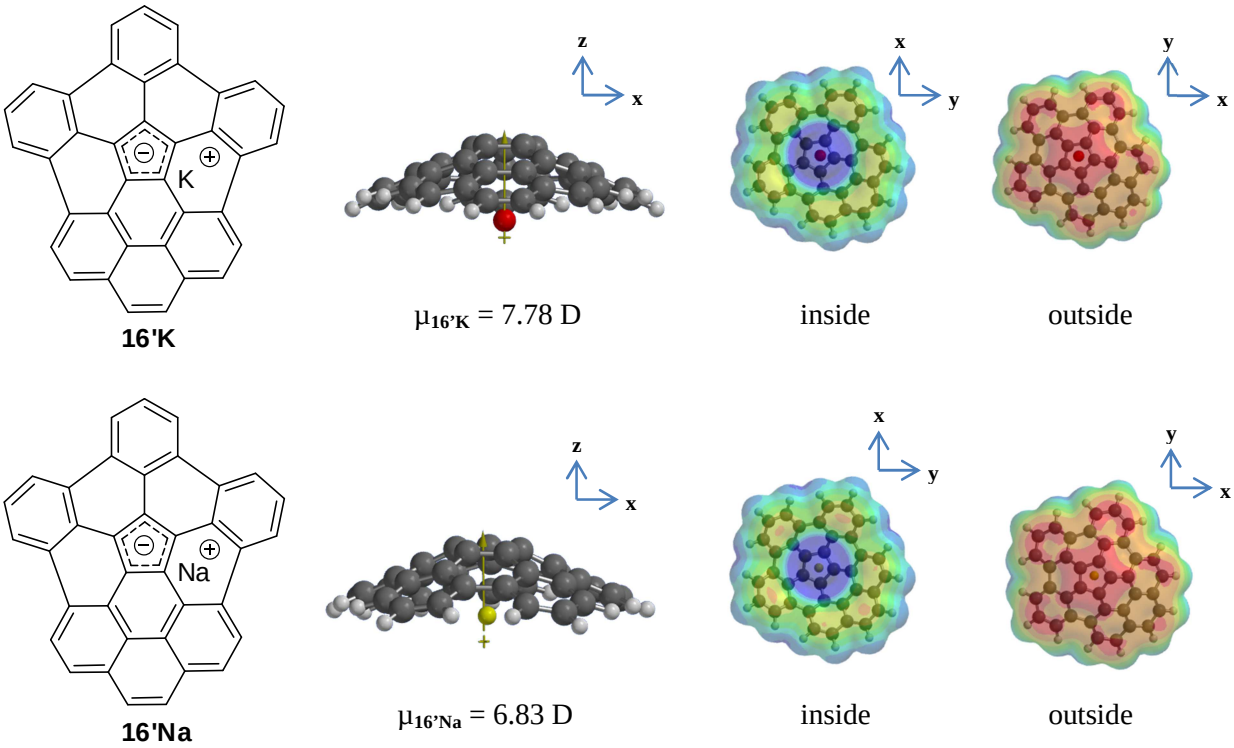

Figure 12: *Calculated dipole moments and electrostatic potential surfaces of* ***16'K*** *and* ***16'Na***

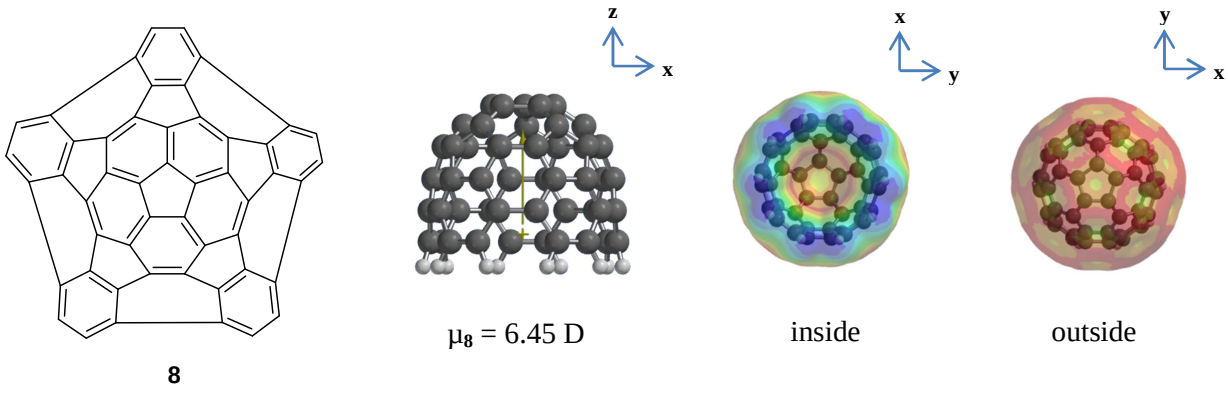

Figure 13: *Calculated dipole moment and electrostatic potential surface of* ***8***

Even if **8** appears to be quite more suitable for hydrogen adsorption due to its apparent higher available adsorption surface, **16'K** and **16'Na** are believed to be even better candidates. Indeed, cations would not only increase or equal the dipole moment of **8** but could also act as spacers between curved PAHs, thus expanding the ILD. The distances measured between the potassium ion and the central pentagonal unit of curved molecule was slightly higher (2.94 Å) than the one between sodium (2.62 Å), making **16'K** the preferred alternative as hydrogen storage material. In *Table 1*, curvature of **8**, **16**, **16'K** and **16'Na** were qualitatively measured by taking the dihedral angle between peripheral carbons and the cyclopentadiene unit (*Figure 14*).

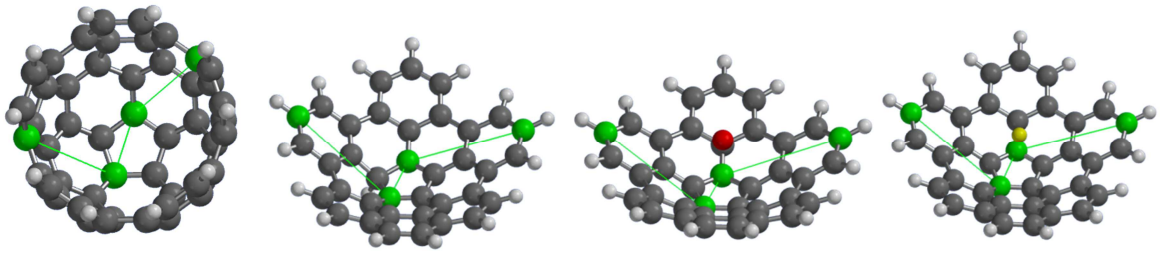

Figure 14: *Dihedral angles for* ***8***, ***16***, ***16'K*** *and* ***16'Na*** *represented in green.*

Curved polyarene	Dihedral angle [°]	Dipole moment [D]
8	64.0	6.45
16	133.0	2.25
16'K	137.1	7.78
16'Na	136.9	6.83

Table 1: *Dihedral angles and dipolar moment for* ***8***, ***16***, ***16'K*** *and* ***16'Na***

Dihedral angles show that from **8** to **16** there is a high decrease in curvature resulting in the lowering of the dipole moment. However, even if the curvature of **16'K** and **16'Na** is of the same order as the one of **16**, the dipole moment is considerably higher due to ionic interactions.

2.2 First strategy starting from 2,6-difluorophenylacetic acid

The first synthetic pathway which was considered starts with the synthesis of 1,3-bis(2,6-difluorophenyl)propan-2-one **13b** from the corresponding carboxylic acid. Compound **13b** will be further reacted with pyrene quinone by a double Knoevenagel condensation followed by addition of phenyllithium and finally, its reduction with $LiAlH_4$. The fluorinated triphenylcyclopentapyrene **15b** will be reacted with γ-Al_2O_3 offering the cyclized molecule by loss of HF [30,31,39] (newly formed C-C bonds). The last step will be the deprotonation of the molecule using KH yielding a potassium complex. It's believed that KH would be a better candidate than NaH (*see* **2.1**). The overall strategy is shown on *Scheme 10*. The first step *i)* was more critical than firstly assumed and the following sections claimed to find appropriate conditions.

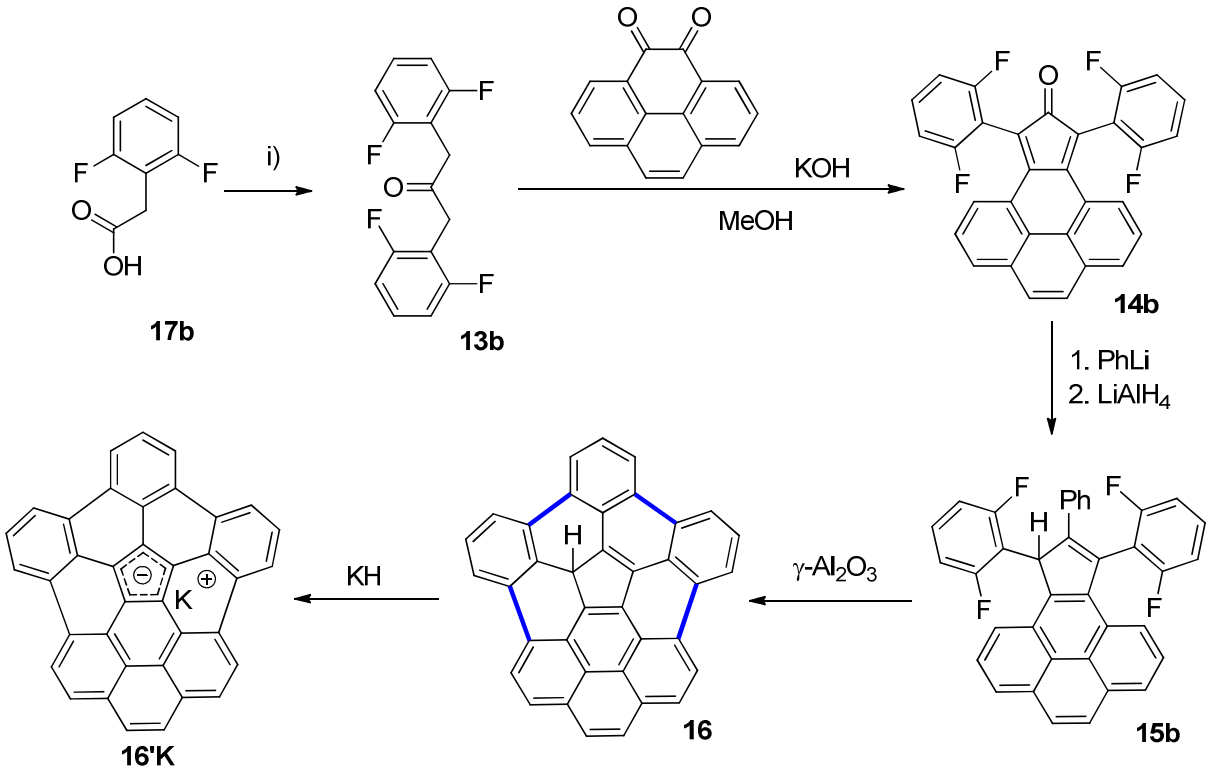

Scheme 10**: Strategy for the synthesis of **16'K** starting from acid **17b

2.2.1 Dakin-West reaction

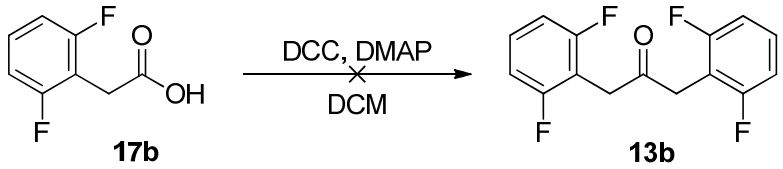

Scheme 11**: Dakin-West reaction of **17b

The Dakin-West reaction was initially used for the preparation of peptides starting from acid and amine precursors, but when it was carried out at room temperature instead of 0 – 4°C by Bhandari in 1998 [40], acid-amine coupling wasn't observed but a symmetrical bisbenzyl ketone was formed instead. Until its discovery, this reaction has been used many times for the synthesis of symmetrical ketones starting from acid precursors. The general procedure used was the following [41] : compound **17b** was added to a coupling agent DCC and DMAP in DCM. Surprisingly in our case, a complex mixture of side products and no traces of **13b** was observed by GC-MS analysis of the reaction medium. Even with slightly modified conditions (*Table 2*) no increase in total efficiency was observed. Indeed, traces of **13b** were observed by GC-MS during the reaction but after filtration to eliminate DCU and acidic extraction removing the DMAP catalyst, many side products with no traces of **13b** anymore were observed. Low temperature didn't show any difference in mixture composition.

	Coupling agent	**Conditions**	**Final yield**
A [40]	DCC	R.t., 1 night	0%
B [42]	EDC	R.t., 1 night	0 %, traces during rxn
C	EDC	-78 °C, 1 night	0 %, traces during rxn

Table 2: *Reaction conditions tested for the Dakin-West reaction*

The reason of such a bad result may be explained by the high electronegativity of the four fluorines in *ortho*-position affecting the methylene reactive center in such a way that a possible charge can be stabilized *via* inductive effects, widening the necessary time for eventual rearrangements; a difficulty encountered with this reaction is that the full mechanism is still not well known and the only proposed mechanism postulated by Bhandari S. et al. seems to be not realistic since the active species **17'** is the result of a highly improbable deprotonation in α of an acid group (*Scheme 12)*.

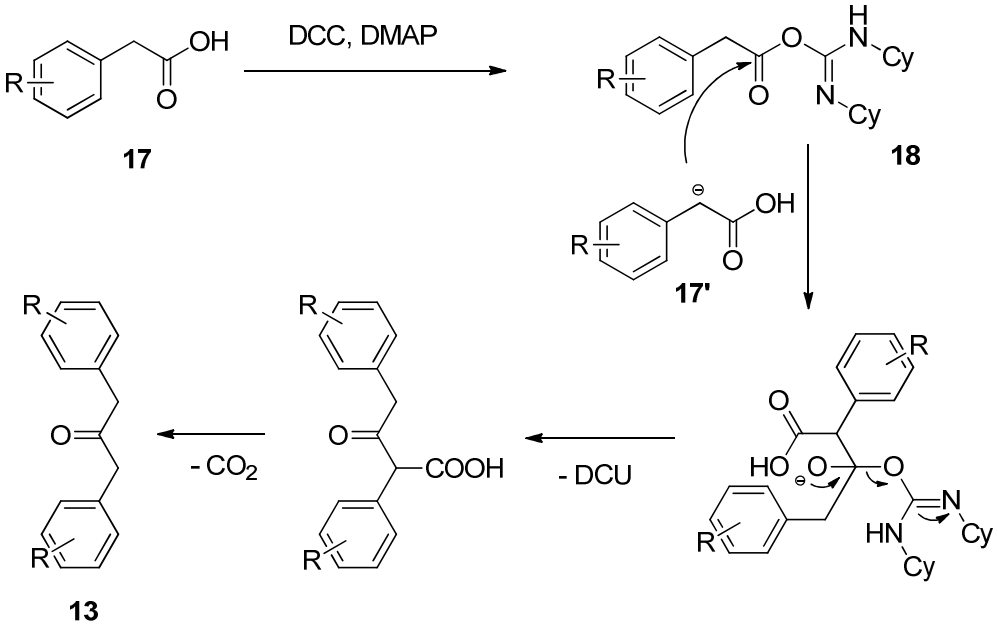

***Scheme 12**: Bhandari et al. proposed mechanism of the Dakin-West reaction*

ESI-MS analysis and computational investigations were further undertaken in chapter **2.3.2** to propose a more probable mechanism.

2.2.2 Ketonic decarboxylation

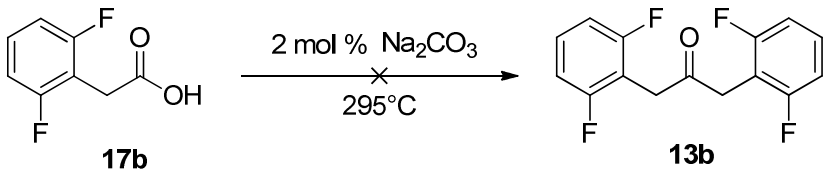

Scheme 13**: Ketonic decarboxylation of **17b

The ketonic decarboxylation is a very old thermic reaction used for the formation of symmetrical ketones and even for the formation of cyclic ketones from dicarboxylic acids [43,44]. However, to our knowledge, such reaction conditions had only been applied to compounds bearing carboxylic acid as their unique functional group. Even so, because fluorinated compounds are known to show high thermal and chemical stability [45], this strategy was tested. Sodium carbonate, used as mild base catalyst was mixed with **17b** and heated at 295°C. Unfortunately a mixture of many side products with no trace of **13b** was observed *via* GC-MS of the crude reaction medium. It seemed that **17b** was more sensible to high temperature than thought in the beginning.

2.2.3 Claisen condensation

Claisen condensation reaction was thought to be the method of choice for the synthesis of **13b** because of the milder reaction conditions as compared to those of ketonic decarboxylation and better knowledge of the mechanism as compared to Dakin-West reaction. The method developed by Romer

et al. [46] allowed the formation of 1,3-diphenylacetone in excellent yield. However this approach adds an extra synthetic step to form the corresponding ester required for the condensation.

Esterification of 2,6-difluorophenylacetic acid [47]

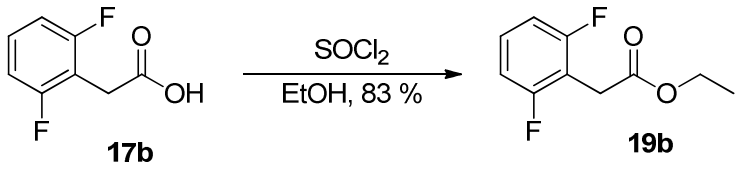

Scheme 14: *Esterification of* ***17b***

Esterification was accomplished by mixing thionyl chloride with **17b** in EtOH and by heating the reaction mixture to reflux during four hours. Evaporation of EtOH and extraction with DCM gave **19b** in 83 % yield. The use of thionyl chloride allowed a quicker reaction by first forming the acyl chloride making the carbonyl carbon more nucleophilic thus favoring ethanol attack to give **19b**. The structure of the ester product **19b** was confirmed *via* mass spectrometry and NMR analysis where an additional triplet and quadruplet corresponding to the ethyl group were observed as well as the disappearance of the O-H vibration (3100 cm^{-1}) in IR spectrum.

Ester condensation of ethyl 2-(2,6-difluorophenyl)acetate

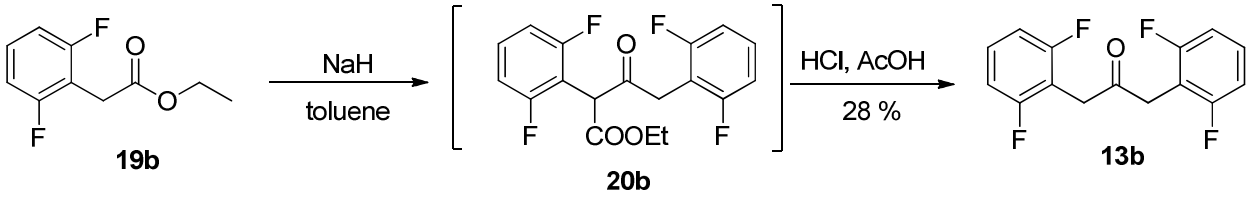

Scheme 15: *Claisen condensation of* ***19b*** *followed by decarboxylation of* ***20b*** *giving symmetrical* ***13b***

Ethyl phenylacetate **19b** was added to NaH in toluene at room temperature and the reaction mixture was heated during one hour. The mixture was then allowed to cool down and quenched with HCl. The mixture was then heated under acidic conditions in order to decarboxylate. Extraction with DCM afforded 28 % of **13b**. ^{13}C-NMR analysis revealed the characteristic downfield shift of the keto-group at *200.1 ppm* while the methylenic protons signal shifted downfield from *3.76 ppm* to *3.91 ppm*. Simultaneously the absence of ethyl signals confirmed the formation of bisbenzyl ketone **13b**. But the low unsatisfactory yield let us look for the structure of side products in the acidified aqueous basic layer. The main product among acetic acid used during decarboxylation step was identified to be acid **17b**. This allowed us to think that the crucial step could be the acidic quenching of **20b** since retro-Claisen might occur. This side reaction was already observed by Romer et al. when quenching was achieved at relatively high temperature (>30 °C) but has been completely avoided at lower temperature [46]. Indeed, under the initial alkaline conditions at the beginning of the quench, the β-keto

ester is hydrolyzed to the β-keto acid, which undergoes a retro-Claisen reaction rather than decarboxylation at high temperatures (60°C) (*Scheme16*).

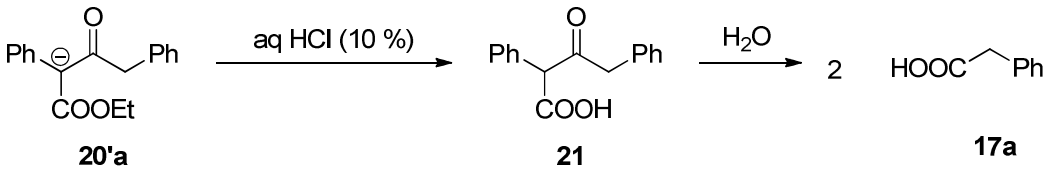

Scheme 16: *Retro-Claisen reaction of **20'a** giving 2 equivalents of **17a***

However, even for a quenching at 0°C, retro-Claisen was observed in our case maybe due to the fluorine atoms making the carbonyl reaction center more electrophilic.

2.3 Second strategy starting from 2,6-dichlorophenylacetic acid

Species synthesized by Thilgen using the HF elimination strategy (*see* **1.4**) did not imply highly curved geometries suggesting that such techniques are not appropriate for extremely curved molecules. [32] Synthesis of strained **16** would necessitate four ring closures in one step to introduce curvature. That's why FVP method or palladium catalyzed Suzuki reaction were considered for the ring closure of chlorinated precursors. [28] Moreover, the new pathway was designed in such a way that a step involving phenyllithium addition on cyclopentadienone derivative followed by reduction was avoided. Indeed, this reaction had already been realized by Weber (*see* **1.4**) starting from **14a** but really small amounts of **15a** with **22** and **22'** as major side products were obtained (*Scheme 17*).

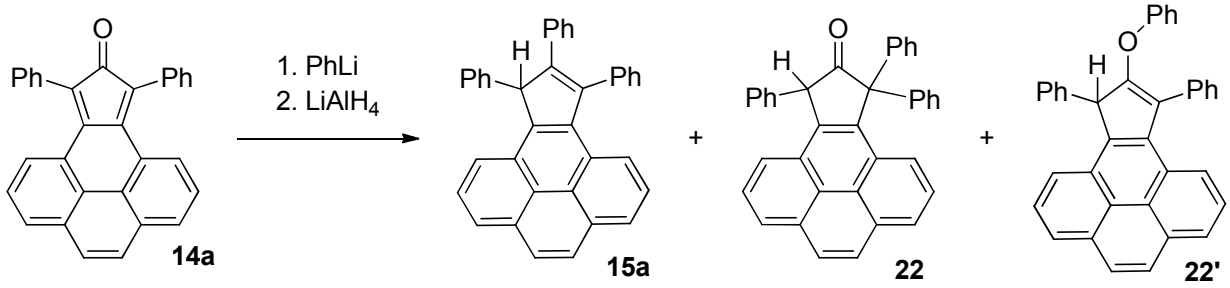

Scheme 17: *Crucial step previously observed by Weber P.; desired **15a** was only observed as minor product*

In the newly proposed pathway, cyclopentadienone derivative **14c** would be condensed with tosyl hydrazine followed by elimination of the tosyl group under basic conditions offering the diazo compound **24** which can react with benzyne to give phenyl dibenzo-indenopyrene **25**, or further reduced providing phenyl dibenzo-indenopyrene **26**. Another advantage of such a new strategy is that one site will already be closed (in red). Finally, compound **26** will be subjected to flash vacuum pyrolysis or Suzuki reaction to close the three remaining rings (in green). The overall strategy is shown on *Scheme 18*. Unfortunately step *i)* was here again more critical than thought and the following sections would claim to find efficient synthetic strategies.

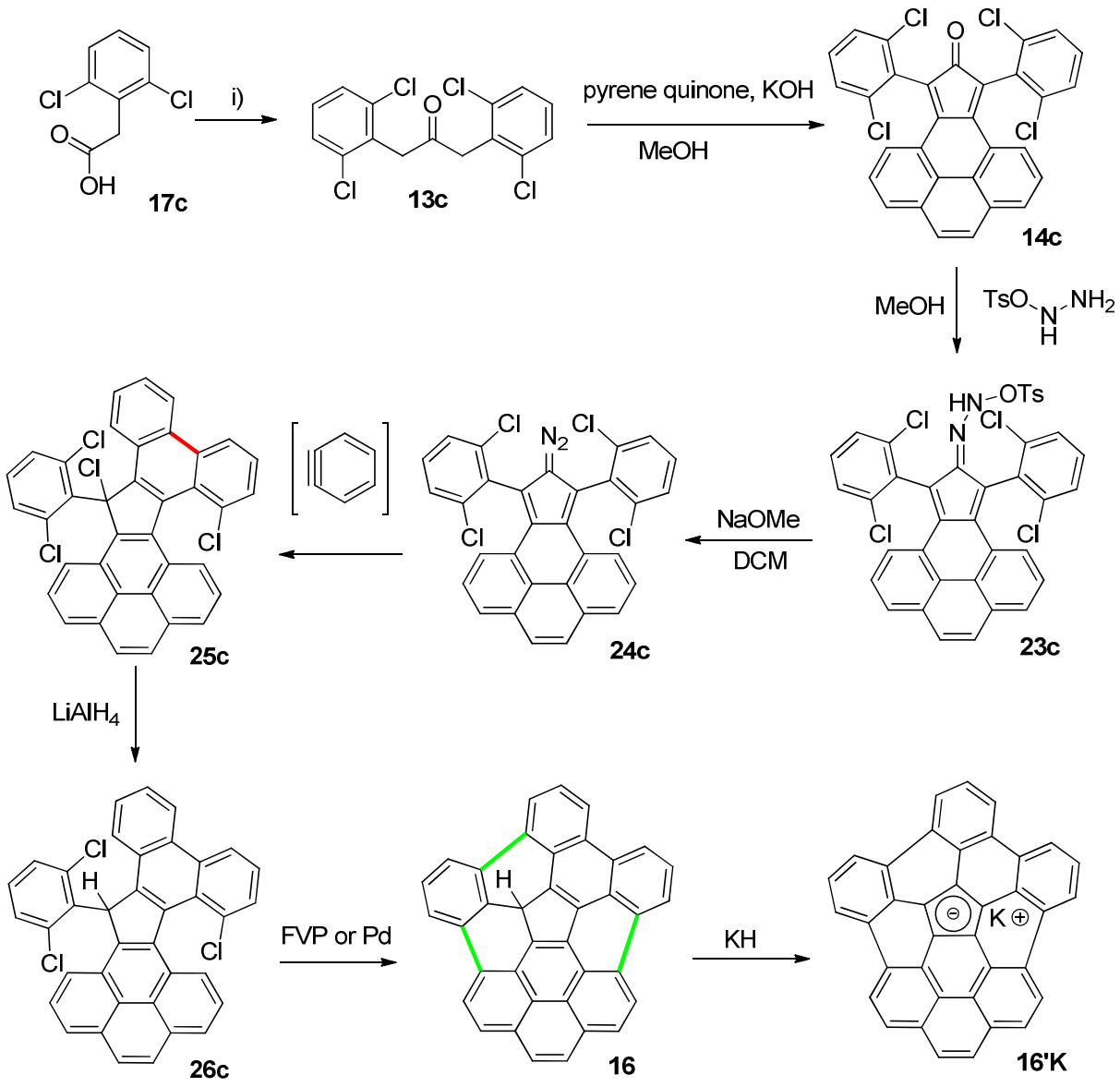

Scheme 18**: Strategy for the synthesis of **16'K** from the acid **17c

2.3.1 Dakin-West reaction

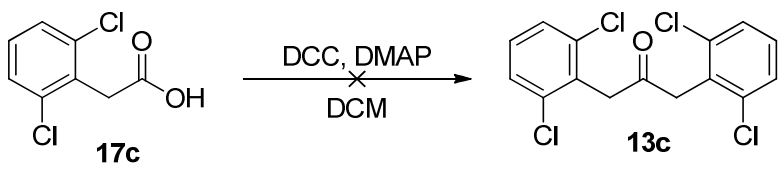

Scheme 19**: Dakin-West reaction of **17c

The same procedure as followed under **2. 2. 1** was used. Reaction conditions tested are summarized in *Table 3*.

	Coupling agent	Base catalyst	Conditions	Solvent	Final yield
A [40]	DCC	DMAP	R.t., 1 night	DCM	0 %
B	DCC	DMAP	R.t., 1 night	THF	0 %
C	DCC	MIM	R.t., 1 night	THF	0 %
D	DCC	Et_3N	R.t., 1 night	THF	0 %
E [48]	DCC	DMAP	56°C, 3h	THF	0 %, but traces during rxn

Table 3**: Conditions tested for Dakin-West reaction of **17c

Traditional procedures [40] gave again no trace of **13c** and because of the very small solubility of **17c** in DCM, it was decided to try the reaction in THF. Here again no traces of **13c** were observed. The substitution of DMAP by MIM or the less nucleophilic triethylamine didn't give better results. Finally, conditions used by Ho et al. for the coupling of *ortho*-nitro derivatives were tested. [48]

Traces of **13c** were observed but in a too small amount and with so many side products that purification was not attempted. For the five reaction conditions, a main product of *286 amu* was identified *via* GC-MS. It may correspond to amide **27c** but no further investigations to characterize and isolate it were undertaken (*Figure 15*).

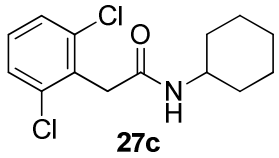

27c

***Figure 15**: Possible structure of the main side product of Dakin-West reaction*

Due to those unsatisfactory results, it was then decided to apply reaction conditions **A** to phenylacetic acid **17a** to see whether 1,3-dibenzylacetone **13a** could be synthesized by this way, as previously reported in literature where yields of roughly 60 % were obtained (*Scheme 20*). [40, 49] This will allow us to see if the bad results for **17b** and **17c** were due to human factors or if it was the consequence of reactivity changes induced by the halogens in *ortho*-position.

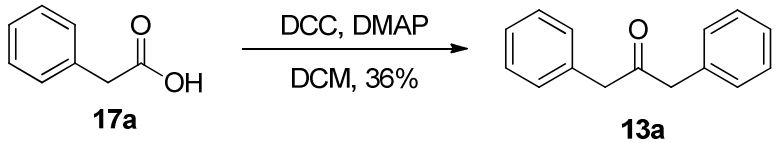

17a **13a**

Scheme 20**: Dakin-West reaction of **17a

The procedure used by Fragnière was used and compound **13a** was obtained as a light yellowish solid (oil at room temperature) in 36 % yield. This low yield suggested that hidden parameters could have unsuspected importance. The structure of **13a** was confirmed thanks to mass spectrometry, ^{13}C-NMR spectroscopy showing a characteristic chemical shift of *205.68 ppm* for the carbonyl carbon and ^{1}H-NMR analysis where methylenic protons shifted downfield from *3.66 ppm* to *3.72 ppm*.

The many intermediates detected by UPLC-ESI-MS during the reaction suggested that several equilibria were involved, making the control of the reaction parameters very tricky. Indeed, the presence of ions (for example, depending on the glassware washing process) could for example stabilize some charged intermediates, thus completely changing their distribution. The variation of ambient temperature may also have a considerable impact on equilibria.

In the following section, the reaction was followed by ESI^+-MS analysis in order to allow identification of the intermediates involved and to postulate a possible reaction mechanism.

2.3.2 Investigations on Dakin-West mechanism

Even if the Dakin-West reaction is now widely used for the synthesis of symmetrical ketones, the mechanism is still not well known and very different yields are reported in literature suggesting that many parameters may affect the reproducibility of the experiment. [33] Attempts to elucidate the mechanism by ESI^+-MS analysis supported by computational calculations were undertaken following the method recently used by Dalla-Vechia et al. [50] for the mechanism elucidation of analogous Dakin-West peptide synthesis.

2.3.2.1 Postulated mechanism based on ESI^+-MS analysis

A possible reaction pathway is postulated on *Scheme 21*. After the molecule numbers, letters **a**, **b** or **c** were added corresponding to X = H, F or Cl. UPLC ESI^+-MS analysis of the crude reaction mixture were undertaken during the reaction of **17a** with DCC and DMAP.

Starting acid **17a** and DMAP were detected in the UV spectrum and a mass range of *150 – 600 amu* in positive detection mode was used. Adduct **18a**, anhydride **28a**, DCC, DCU and acylamide cation **29a** were all observed *via* ESI^+-MS during the mixing of the starting reagents (*Table 4*).

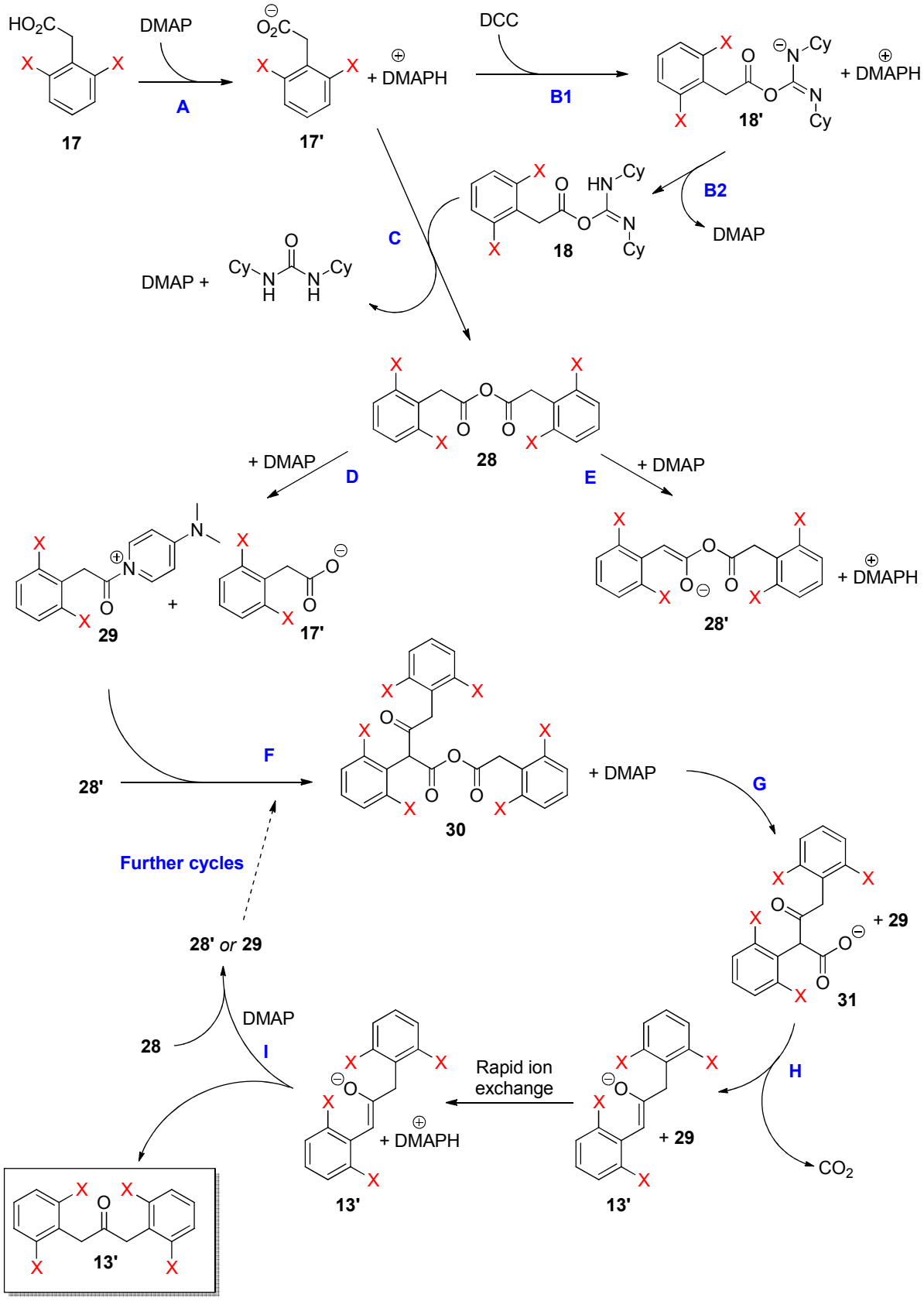

Scheme 21: *Postulated Dakin-West mechanism based on ESI$^+$-MS analyses*

After only fifteen minutes, the desired bisbenzyl ketone **17a** was observed with a complex mixture of side products where DCU, DMAP, anhydride **30a**, amide **27a**, diketone **32**, enol ester **32'** and N-acylium **33** were the solely identified structures (*Figure 16*). No mechanism was found to explain the formation of **27a**, but **32** and **32'** should result of the reaction between **13'a** and **29**. Cation **33** would be probably produced after the nucleophilic attack of **30** by DMAP on the most hindered carbonyl group.

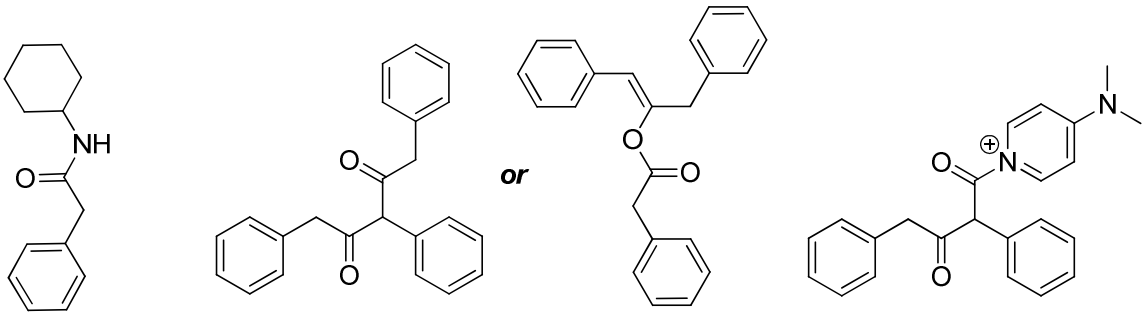

27a **32** $C_{23}H_{20}O_2$ **32'** $C_{23}H_{20}O_2$ **33**

Figure 16: *Additional identified structures observed after 15 minutes*

Molecule M	ESI-MS: *m/z*	Corresponding ion
17a	*211.14*	$[M+H]^+$
27a	*218.20*	$[M+H]^+$
30	*373.26*	$[M+H]^+$
32	*329.22, 351.13, 392.17*	$[M+H]^+$, $[M+Na]^+$, $[M+Na+ MeCN]^+$
33	*359.23*	$[M]^+$

Table 5: *Species detected by ESI$^+$-MS after 15 minutes*

After 24 hours, the crude mixture composition had not evolved suggesting that key steps were at the really beginning of the reaction before thermodynamical equilibration occurred. The presence of DMAP at the end of the reaction proved its role of catalyst.

2.3.2.2 Computational calculations on the Dakin West reaction intermediates

Computational calculations were performed at the B3LYP level using the PCM solvation model [51] available in the Gaussian09 package in order to corroborate the feasibility of the reaction. B3LYP/6-31G* geometry optimizations were done in DCM by following the same procedure as those used under **2.1**. Single point energy calculations at HF/3-21G were done on the optimized structures using Spartan 10' for visualization of the orbitals. The whole charged structures were computed with their corresponding counterion in order to handle a neutral system. The electrostatic energy potential surfaces of all the charged structures were computed to see where the counterion is preferably located.

Each step of the postulated mechanism described in *Scheme 21* was considered separately. If there were many possibilities for a step, the most probable pathway was chosen according to the calculated Gibbs reaction enthalpies and the qualitative concentration of reactants in the reaction media. Chlorinated compounds were also calculated to see which step could be critical.

Step A

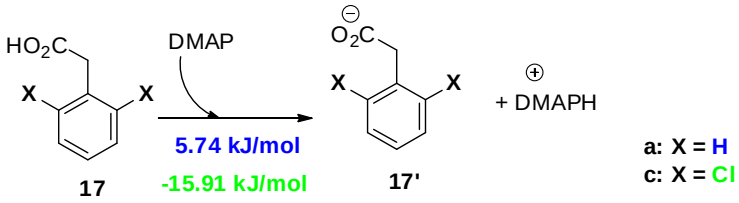

Scheme 22: *Deprotonation of* ***17***

The Gibbs reaction enthalpy of **17a** showed that even if the reaction is found to be slightly endothermic, the energy barrier is so low that it can easily be overcome at room temperature. For **17c**, the reaction was found to be spontaneous. This difference is due to an important change of the dihedral angle **4 – 7 – 8 – 12** from 60.67 ° in **17'a** to 3.3 ° in **17'c** (*Figure 17*).

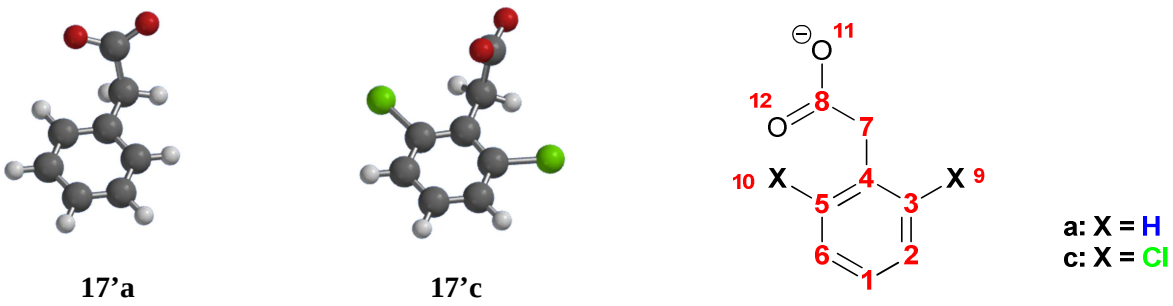

Figure 17: *Geometry changes of acetate group between* ***17'a*** *and chlorinated* ***17'c****. Numbering of atoms for Mulliken charges assignment achieved in Table 6*

This geometry difference would be the result of a better electrostatic stabilization of carboxylate in the second case as illustrated by the calculated Mulliken charge distribution (*Table 6*).

Atom	Mulliken charges [a.u.]	
	X = H (**17'a**)	X = Cl (**17'c**)
1	-0.09	-0.04
2, **6**	0.03	-0.11
3, **5**	-0.09	0.49
4	0.20	-0.02
7	-0.14	-0.18
8	1.45	1.55
9, **10**	0.00, 0.07	-0.44
11	-1.10	-1.06
12	-1.13	-1.21

***Table 6**: Mulliken charges of **17'a** and **17'c** computed from B3LYP/6-31G* calculations*

The main difference was noticed at carbons **3** and **5** where strongly positive Mulliken charges in **17'c** were observed due to the presence of adjacent electronegative chlorine atoms. This would lead to electrostatic attraction with the acetate anion. Furthermore, maximal electrostatic repulsion between chlorines and negatively charged oxygen would also favor this geometry.

In *Figure 18*, planar interactions between the LUMO of $DMAPH^+$ with HOMO of the carboxylate are illustrated.

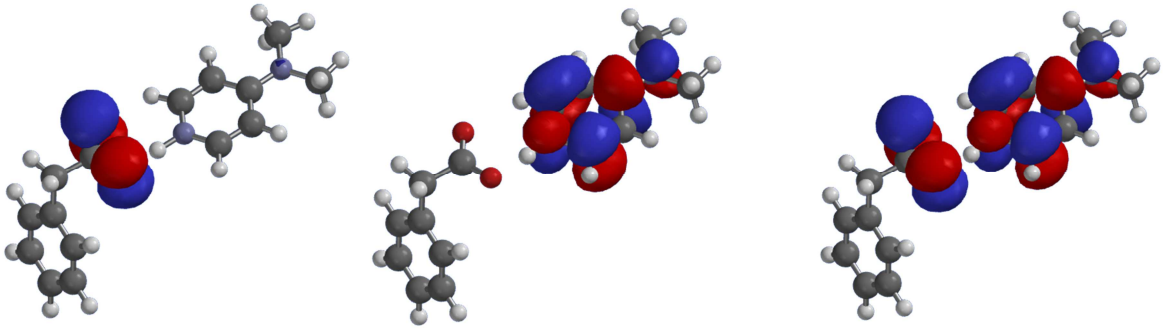

***Figure 18:** From the left, HOMO, LUMO and HOMO-LUMO interaction of ion pair **17'a** – $DMAPH^+$*

Step B

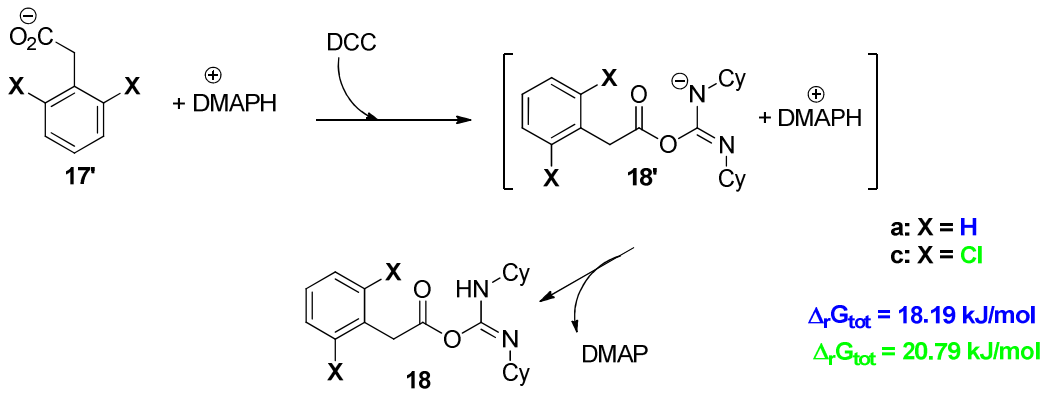

Scheme 23: *Formation of* ***18*** *starting from* ***17'*** *and DCC*

This reaction step is quite endergonic giving rise to roughly 0.02 % of **18'**, but because the next step is highly exergonic, **18** will be immediately consumed. Therefore with enough time, this activation barrier would probably be overcome. However, experimental observations showed that production of DCU (*Step C*) was instantaneous and this tells us that there must be a small discrepancy between calculations and real experiments. One might be closer to the experimental value by explicitly modeling the solvent molecules but this would considerably increase the time of calculations.

When geometry optimization of the ion pair **18'** – $DMAPH^+$ was run, they immediately combined releasing **18** and DMAP. This would suggest that the reaction was concerted; a possible transition state is postulated in *Figure 19*.

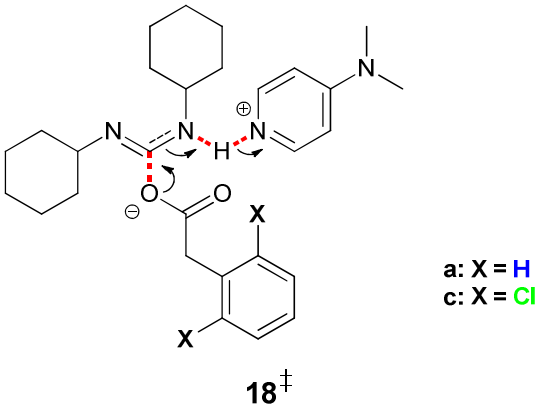

Figure 19: *Possible transition state for the reaction between* ***17'****,* $DMAPH^+$ *and DCC releasing* ***18*** *and DMAP*

No transition state calculations were investigated due to the arduous procedure for such researches.

Step C

Two possible reactions were investigated. Each of them was strongly exergonic. Gibbs reaction enthalpies are of the same order between **28a** and **28c** formation, except in the second possibility in

which **28c** formation is less favored. As already found in *step A*, this will be due to the higher stability of **17'** in chlorinated compound.

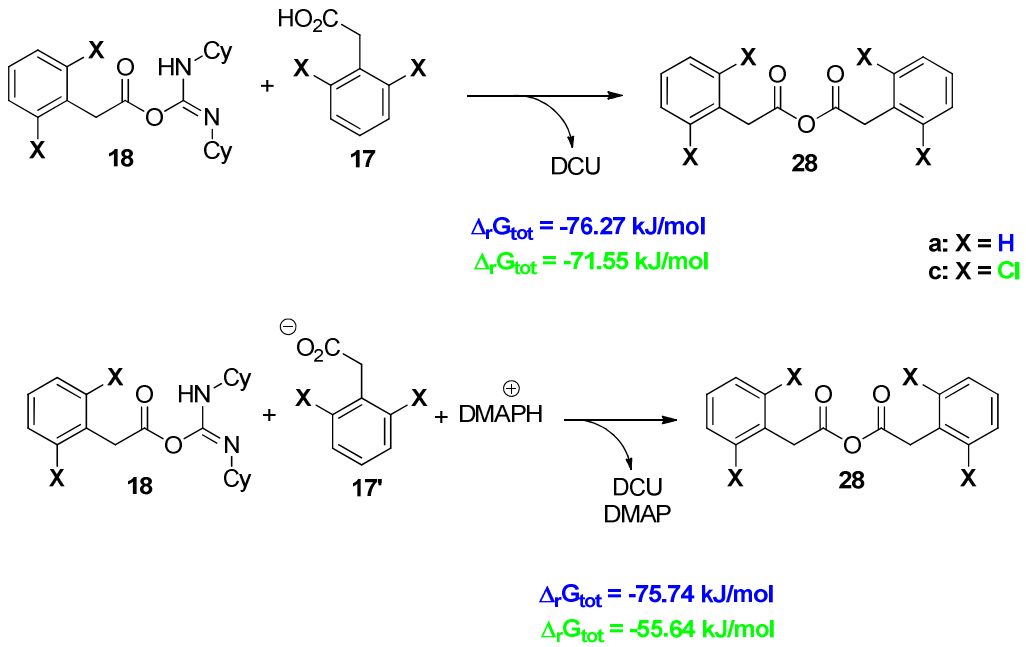

Scheme 24: *Formation of anhydride **28** starting from **18** and **17'** in the first possibility and from **18** and **17** in the second*

Step D

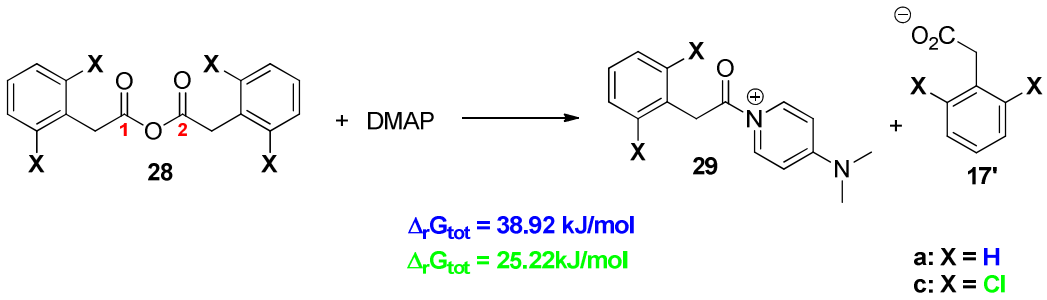

Scheme 25: *Nucleophilic attack of **28** by DMAP*

If anhydride **28** and DMAP were calculated separately, Gibbs reaction enthalpies were too high (72.56 kJ/mol or 57.64 kJ/mol for chlorinated compound). But when calculated together, they looked to be roughly 13 kJ/mol more favorable for chlorinated species. This will be again attributed to the higher stability of **17'**. Furthermore Mulliken charges at centers 1 and 2 were found to be 0.62 a.u. in **28a** and 1.53 a.u. in **28c** making the latter a better candidate for nucleophilic attack. Nevertheless, the reason of such a difference was not really elucidated.

Step E

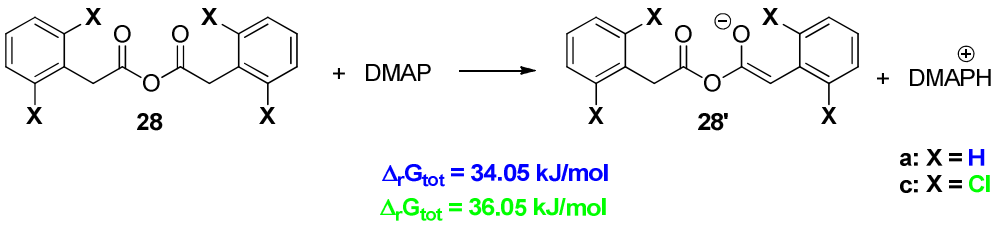

Scheme 26: *Deprotonation of **28** by DMAP*

Here again, the computation of anhydride with DMAP gave better results than separated species. At first, formation of **28'c** was thought to be favored over **28'a** due to inductive effect of the chlorines which should stabilize the negative charge created after deprotonation by DMAP. Nevertheless this trend was not observed and the reaction was found to be even slightly less favorable for **28'c**. Indeed, mesomeric effect should also be considered and resonance structures were drawn below.

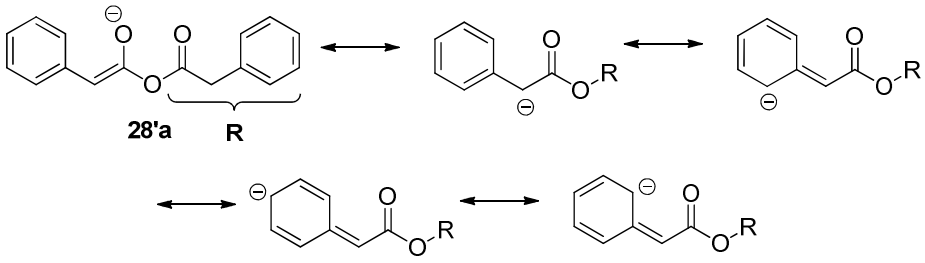

Scheme 27: *Contributing structures for **28'a***

For **28'a**, there were two additional contributing structure compared to **28'c** (*Scheme 27*, *28*). Thus, negative charge was more evenly stabilized in **28'a**.

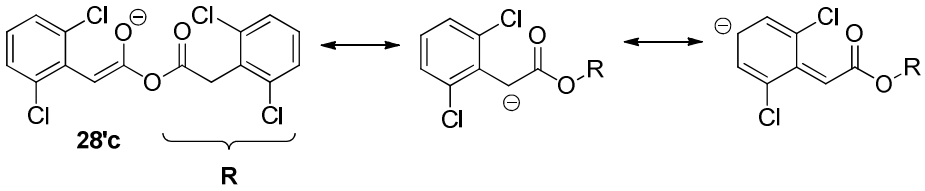

Scheme 28: *Contributing structures for **28'c***

This observation was confirmed by the calculated Mulliken charge distribution (*Table 7*).

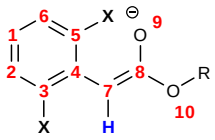

28'

Atom	Mulliken charges [a.u.]	
	X = H (**28'a**)	X = Cl (**28'c**)
1	-0.31	-0.24
2, **6**	0.19	0.03
3, **5**	-0.28	0.28
4	0.72	0.51
7	-1.06	-1.08
8	2.00	2.06
9	-1.16	-1.14
10	-1.49	-1.47

Table 7: *Mulliken charge distributions of **28'a** and **28'c***

Moreover another effect was noticed in the calculated structures. The dihedral angle between **H** – **7** – **4** – **3** was found to be 0.10 ° in **28'a** *versus* 26.45 ° in **28'c**. In the latter, overlap of the anionic p-orbital with π-orbitals of the benzene ring was hindered (*Figure 20*). This may be caused by high electrostatic repulsion between the chlorine atoms and oxygen atom **9**, or simply by sterical hindrance of the substituents in *ortho*-position.

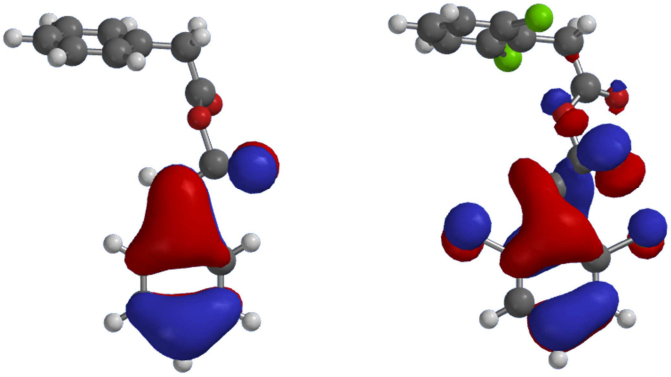

Figure 20: *From the left, HOMO-2 of **28'a** and **28'c** illustrating the overlap of π-MO of benzene ring with p-AO of anion*

Steps D and *E* are in competition and were thought to be key steps. Indeed, if nucleophilic attack was preferred, the reaction would stop at this point. Production of **28'** is absolutely required to follow the desired reaction pathway. When X=H, it was found that Gibbs reaction enthalpy of **E** was slightly preferred, allowing further steps to proceed; When X=Cl, nucleophilic reaction is favored by roughly 11 kJ/mol, thus hindering the production of the active species **28'c**. This might be the reason why the Dakin-West reaction wouldn't work for *ortho*-dihalogenated compounds.

Step F

For the three following postulated possibilities, the counterion of the anionic species is $DMAPH^+$, but omitted in the scheme for clarity reasons.

First possibility

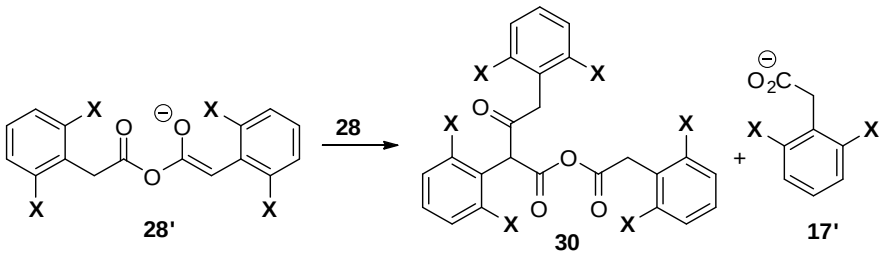

Scheme 29: *Nucleophilic attack of **28** by **28'***

Deprotonated **28'** would react with anhydride **28** to give species **30** with deprotonated acid **17'** and $DMAPH^+$. Surprisingly, there was no big enthalpy difference between **a** and **c** while **17'c** has been found to be more stable in the past steps. Therefore, species **30** would be less stable for chlorinated compound. Electrostatic repulsion between chlorines and oxygen in **30c** (in red) would force the molecule to adopt a geometry in which oxygen atoms are closer (in blue), thus destabilizing the molecule (*Figure 21*). Distance between oxygen decreased from 3.09 Å in **30a** to 2.8 Å in **30c**.

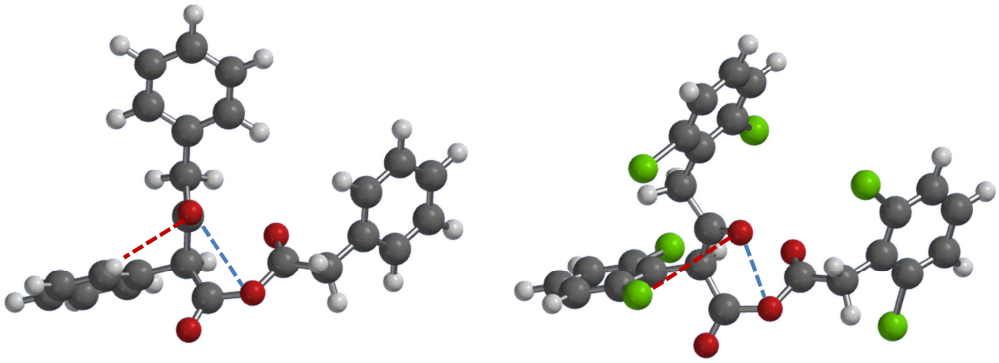

Figure 21: *Destabilisation of **30c** due to electrostatic interactions*

Second possibility

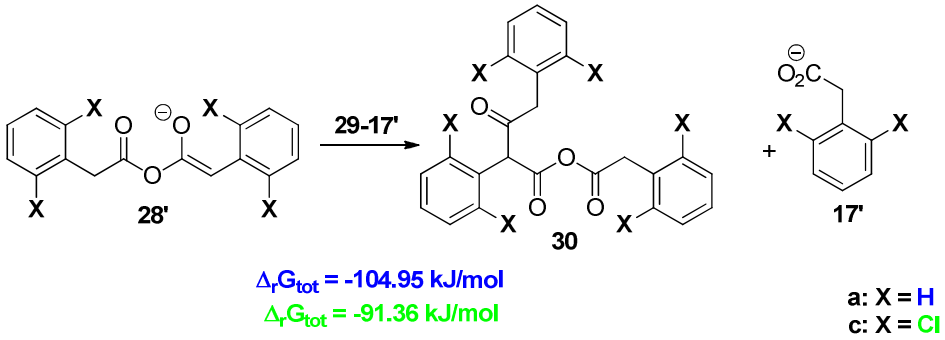

Scheme 30: *Nucleophilic attack of **29** by **28'***

Nucleophilic attack of **28'** on N-acylium **29** formed in *step D* released acetate **17'** and compound **30**.

Third possibility

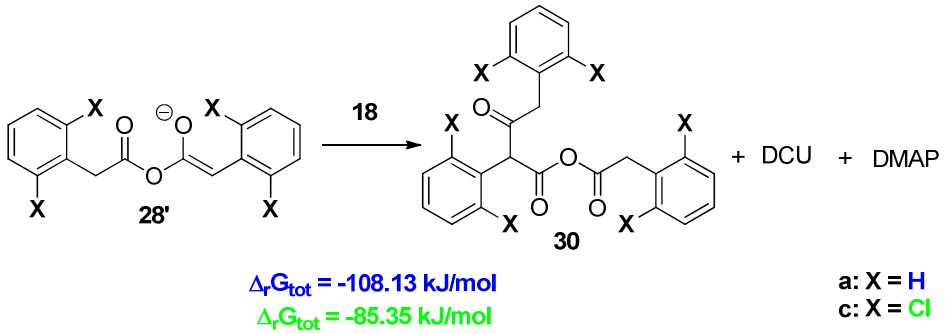

Scheme 31: *Nucleophilic attack of **18** by **28'***

Adduct **18**, formed in *step B* will undergo nucleophilic attack by **28'** producing **30**, DMAP and DCU.

In all possibilities, reactions were found to be exergonic, but in the second case, species **29** was thought to be present in relatively small quantities while adduct **18** and anhydride **28** should be present in higher concentration. Of these two possibilities, the last one presents an advantage, namely the production of DCU which will precipitate and thus strongly favor the reaction.

Step G

The next step was delicate because the base can either abstract a proton releasing a stabilized β-ketoester **30'** or act as a nucleophile (*Scheme 32*).

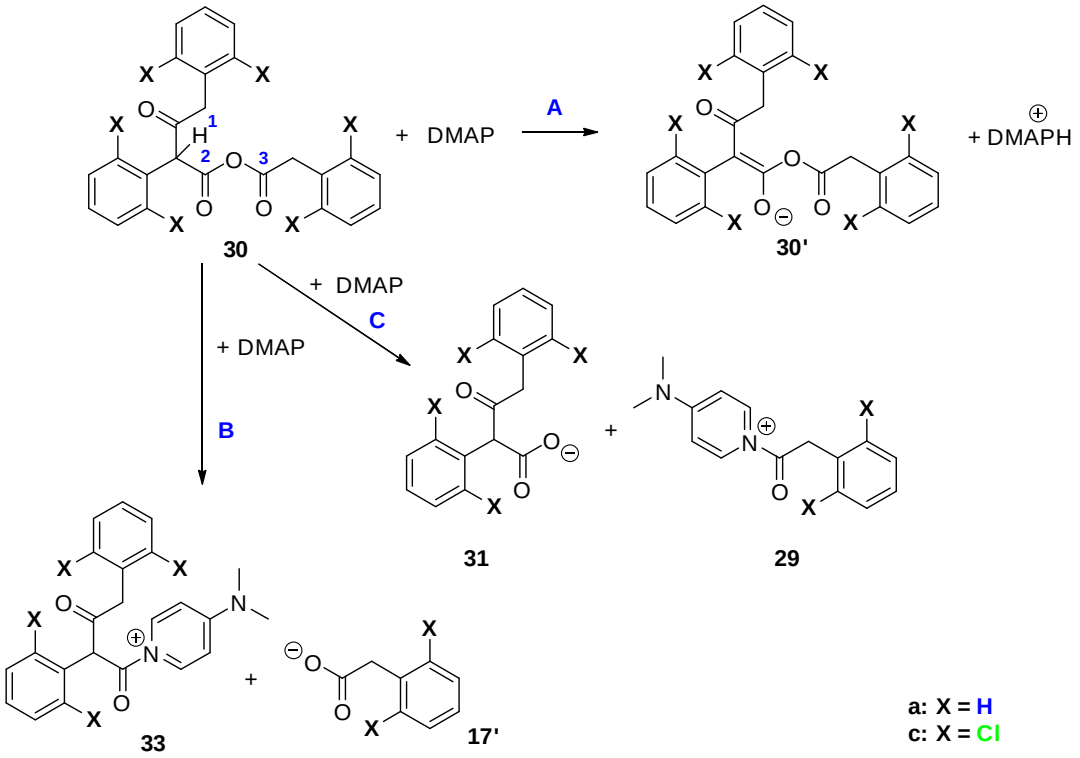

Scheme 32: *Deprotonation of **30** by DMAP (**1**) and nucleophilic attack on (**2**) or (**3**)*

Normally, the first case would happen but in the computed electrostatic energy surface, it can be seen that at center 1 there would be highly sterically hindred due to oxygen atoms and the phenyl substituant (*Figure 22*); thus DMAP would probably better act as a nucleophile. Even if **B** could also happen (traces of **33** were observed in ESI^+-MS analysis), the reactive center of choice should be 3. **C** was the only possibility which was considered (*Scheme 33*).

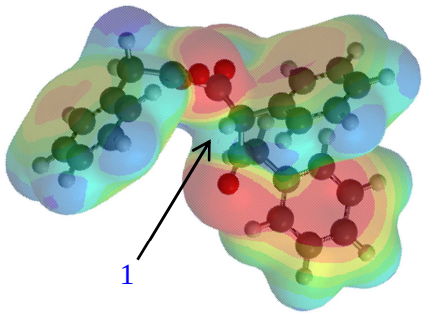

Figure 22: *Electrostatic potential surface of **30c***

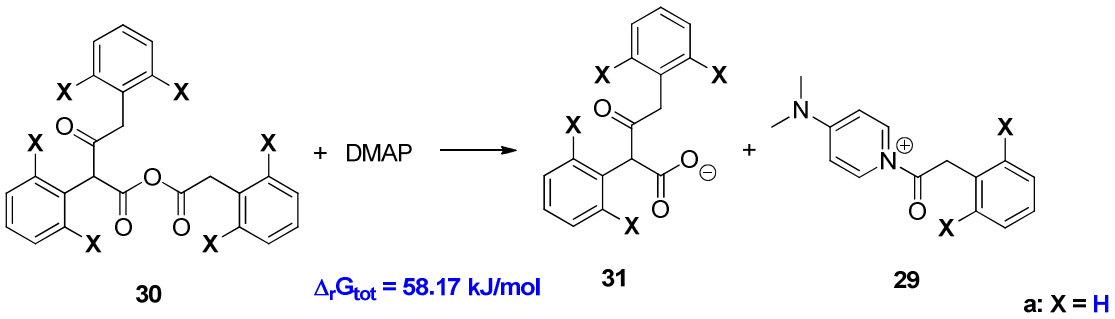

Scheme 33: *Nucleophilic attack of **30** by DMAP*

Unfortunately, the Gibbs reaction enthalpy which was only computed for **31a** was too high. It should be kept in mind that **30** and the ion pair **31**-**29** would have many degrees of freedom increasing the probability that the calculated energy minimum wouldn't correspond to the global minimum but to a local minimum. No further calculations for finding a better energy minimum were undertaken.

Step H

This decarboxylation step would occur quite easily although not exergonic for chlorinated species. Anyway, gas evolution will push the equilibrium towards product **13'**. Compound **31** was not observed experimentally because the ESI-MS detection mode was positive.

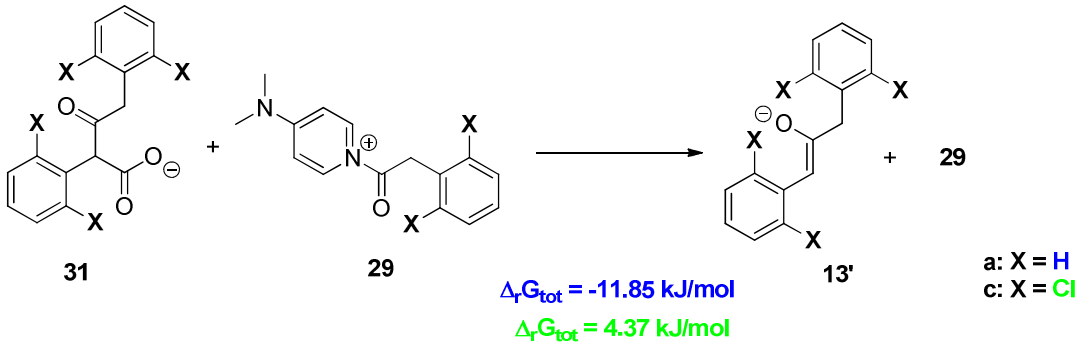

Scheme 34: *Decarboxylation of **31***

At this point, as assumed by Dalla-Vechia L. et al. in their calculations, a fast counterion exchange has been considered (*Scheme 35*).

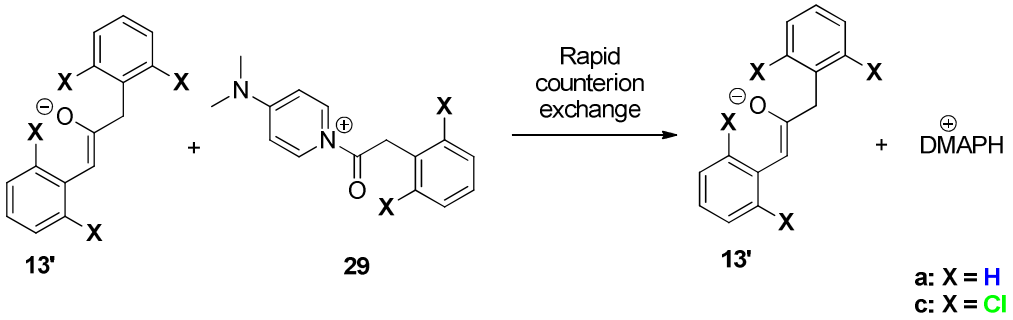

Scheme 35: *Rapid counterion exchange*

However, it should be kept in mind that some species as **29** would not undergo such a counterion exchange but suffer a nucleophilic attack of **13'**. This explains the detection of traces of **32** (see **2.3.2.1**) (*Scheme 36*).

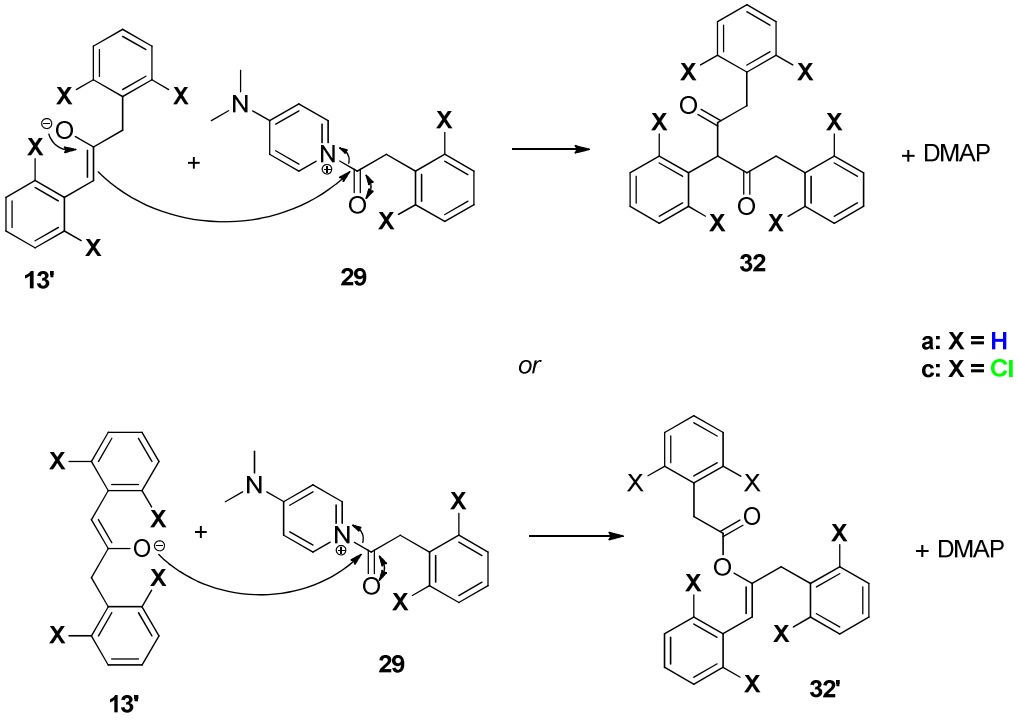

Scheme 36: *Side reactions which could occur before counterion exchange*

Step I

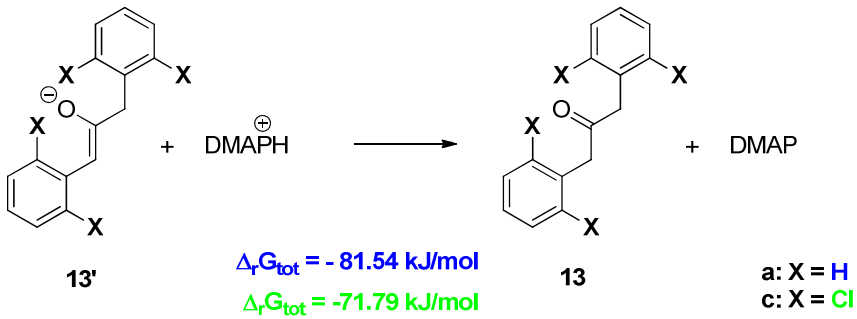

Scheme 37: *Protonation of **13'** to give **13***

Reprotonation of enolate **13'** is largely exergonic in the two cases regenerating the DMAP catalyst.

General considerations

Identification of anhydride **28** as an intermediate gave us the idea to explore another synthetic approach which would first start from the synthesis of anhydride further treated with DMAP to release **13**. In this way, the production of DCU and nitrogen containing intermediates could be avoided and possible amide side product formation as **27a** and **27b** could be avoided (*see* **2.3.1** and **2.3.2.1**). Bhandari et al. have already tried such an approach starting from acyl chloride for the synthesis of

anhydride but without obtaining any trace of **13a**. Despite these poor results, it was decided to test this new pathway.

2.3.3 Anhydride pathway

Based on the work of Tran et al. in which they achieved a variant of the Dakin-West ketone synthesis by the reaction of phenylacetic acid **17a** with acetic anhydride catalyzed by MIM releasing 1-phenylpropan-2-one [52], it was thought that by starting with 2-phenylacetic anhydride **28a**, the desired bisbenzyl ketone **13a** should be obtained.

Anhydride synthesis

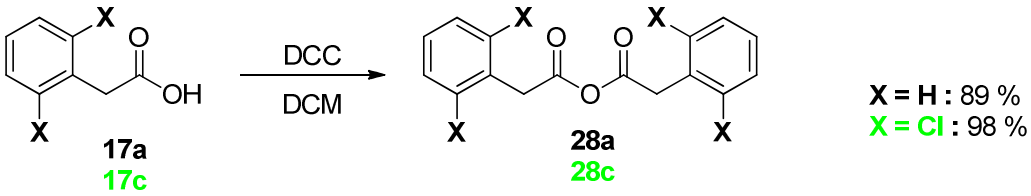

Scheme 38: *Anhydride **28** synthesis starting from **17***

Anhydrides **28** were prepared according to Selinger Z. et al. who synthesized fatty acid anhydrides by the reaction of the corresponding acid with DCC in excellent yields. [53] A solution of **17** was added to DCC in dry DCM and allowed to react. The suspension was filtered and the solvent evaporated. Because DCU is slightly soluble in DCM [54] but really less soluble in MeCN, the obtained white solid was dissolved in the latter at 0°C and filtered removing the remaining DCU. Compounds **28a-c** were obtained as white solids in 89 – 98 % yield. The presence of **28a-c** were confirmed by ^{1}H-NMR where methylenic protons are shifted downfield from *3.66 ppm* in **17a** (*4.08 ppm* in **17c**) to *3.74 ppm* (*4.16 ppm*) and integral values rose from 2H to 4H.

In the ^{13}C-NMR spectrum, a carbonyl carbon signal shifted upfield from around *178 ppm* to characteristic *168 ppm* in **28a** (*164 ppm* for **28c**). The disappearance of the O-H vibration of the acid group **17** at around *3000 cm^{-1}* and the classical two bands for the carbonyl groups of **28** at around *1800* and *1700 cm^{-1}* were observed *via* IR spectroscopy. Masses of *277.09 amu* corresponding to [**28a** + Na]$^{+}$ and *413.03 amu* for [**28c** + Na]$^{+}$ were observed by UPLC ESI^{+}-MS. An acid moiety was also detected but can be attributed to the acidity of the column. Under those conditions, anhydride **28** would partially hydrolyze releasing two acid molecules **17**.

Bisbenzyl ketone synthesis

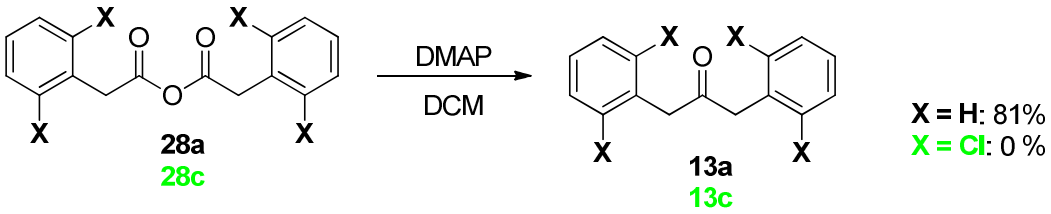

Scheme 39: *Decarboxylation of **28** giving ketone **13***

DMAP was added to **28** in dry DCM and the reaction mixture was stirred during six hours. Thanks to ESI^+-MS of the crude reaction mixture, the formation of **13a** was detected whereas no traces of **13c** were identified. The solution was then quenched by adding HCl and the organic layer was washed with $NaHCO_3$. Compound **13a** was obtained in 81 % yield as yellowish oil crystallizing in the fridge. Identification by mass spectrometry and NMR experiments gave exactly the same results as those obtained under **2.3.1**. The obtained total yield for this anhydride pathway was 72 %, which was really satisfaying. Moreover, this would contradict Bhandari S. et al., which had stated that it was impossible to synthesize **13a** following the anhydride pathway. [40]

Unfortunately, no traces of **13c** were obtained and as predicted in section **2.3.2.2** by the fact that DMAP would rather act as a nucleophile than as a base, thus only producing N-acylium **29c** (*Scheme 40*). ESI^+-MS of the crude reaction mixture gave a mass of *309.06 amu* confirming the presence of **29c**.

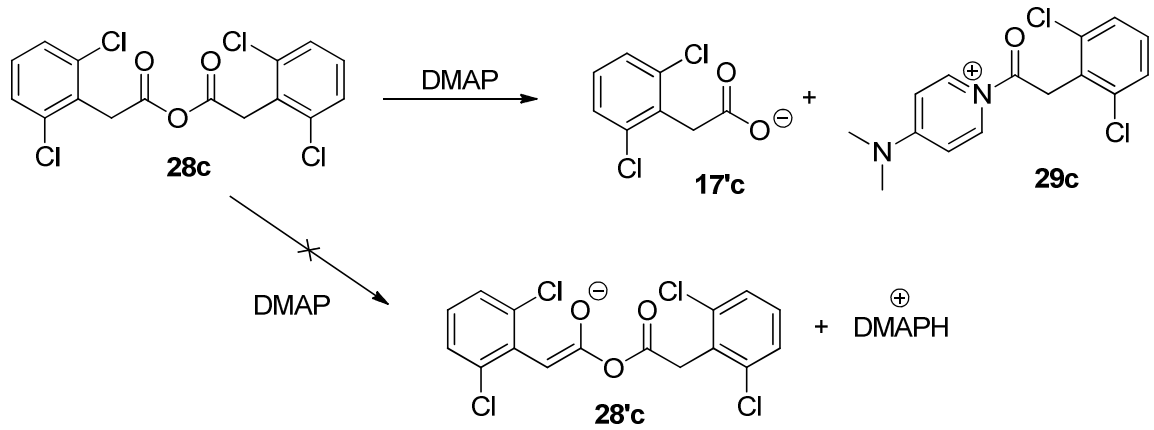

Scheme 40: *Acylium **29c** formation instead of deprotonated anhydride **28'c***

Use of a non-nucleophilic base could favor **28'c** formation. Therefore Hünig's base (DIPEA) was tested instead of DMAP. Its poor nucleophilicity is due to the steric shielding of the nitrogen atom by the ethyl and the two diisopropyl groups, making the lone pair only accessible for a proton. However, no reaction was observed under these conditions. This could be due to the steric hindrance caused by the chlorine atoms which would hinder the approach of DIPEA.

2.3.4 Claisen condensation

Because Claisen condensation gave the best results for **13b**, this synthetic pathway was also tested on the chlorinated compound **17c** to form the corresponding ketone **13c**.

Esterification of 2,6-dichlorophenylacetic acid [47]

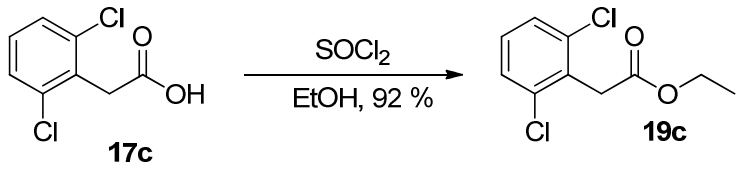

Scheme 41: *Esterification of* ***17c***

The exact same reaction conditions as those followed under **2.2.3** were applied. Esterification of acid **17c** gave **19c** as a white solid in nearly quantitative yield. The structure of **19c** was confirmed by mass spectrometry and ^{1}H-NMR spectroscopy where the expected ethyl signals were detected at *1.24 ppm* and *3.99 ppm*.

Ester condensation of ethyl 2-(2,6-dichlorophenyl)acetate

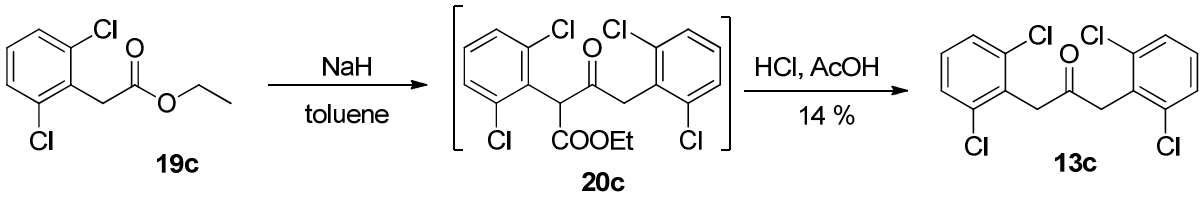

Scheme 42: *Claisen condensation of* ***19c*** *followed by decarboxylation of* ***20c***

Following the procedure as described under **2.2.3**, compound **13c** was obtained as a yellow solid in 14 % yield. This modest result could also be due to the additional steric hindrance due to the chlorine in **19c** as compared to the fluorinated **19a**. This would hinder the approach of another molecule of **19c** near the methylenic center preventing the desired bimolecular reaction. It was thought that maybe the use of LDA as a base should be a good choice. The lithium cation could produce a template effect by coordinating with the carbonyl oxygen of another molecule of **19c** thus bringing closer the two reacting species in a six-member ring transition state (*Firgure 23*).

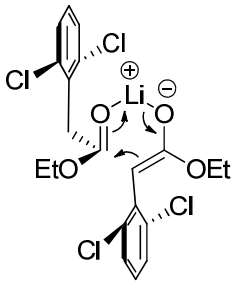

Figure 23: *Possible intermediate species during LDA-mediated Claisen condensation*

Unfortunately these conditions gave no trace of **13c**.

2.3.5 Grignard reaction

According to the difficulty to handle enolates in Claisen condensation, the lack of results obtained *via* anhydride pathway and Dakin-West reaction, another strategy involving the reaction of an acyl chloride with Grignard reagent was developed (*Scheme 43).*

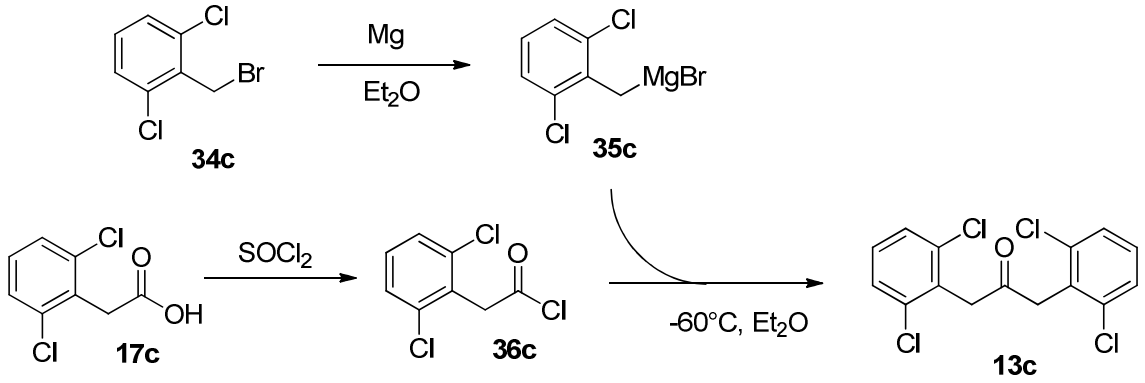

Scheme 43: *Grignard reaction between* ***36c*** *and* ***35c*** *releasing* ***13c***

Acyl chloride **36c** previously synthesized from **17c** was reacted with Grignard reagent **35c** formed through the reaction of compound **34c** with magnesium. This reaction was thought to be less dependent of the methylenic reactive center. Another advantage of this pathway is that preparation of asymmetrical ketones would be possible thus opening the scope of combining chlorinated compounds with fluorinated ones.

Acyl chloride synthesis

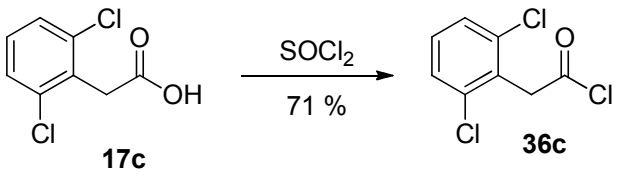

Scheme 44: *Synthesis of acyl chlorid* ***36c*** *from acid* ***17c***

Acyl chloride **35c** was prepared according to Takahashi et al. who prepared triphenylacetyl chlorid in quantitative yield. [55] Compound **17c** was mixed with thionyl chloride and heated to reflux. Compound **36c** was obtained in 71 % yield as a transparent oil. Structure of **36c** was confirmed by mass spectrometry and ^{1}H-NMR analysis, which showed the shift of methylenic protons from *4.08 ppm* in **17c** to *4.54 ppm*. In the IR spectrum, the typical carboxylic O-H vibration at around *3000 cm^{-1}* disappeared giving way to a C-Cl vibration at *609 cm^{-1}*.

Grignard reaction between acyl chloride and Grignard reagent

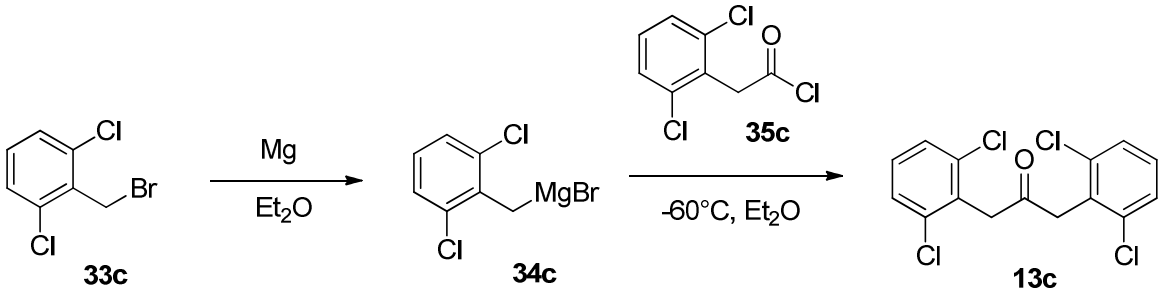

Scheme 45: *Grignard reaction of **34c** with **35c** releasing **13c***

Based on a procedure used by Turro et al. [56], the Grignard reagent was first formed by mixing **33c** with magnesium in Et_2O and then mixed with compound **35c** at low temperature in order to avoid formation of compound **37c** (*Scheme 46*).

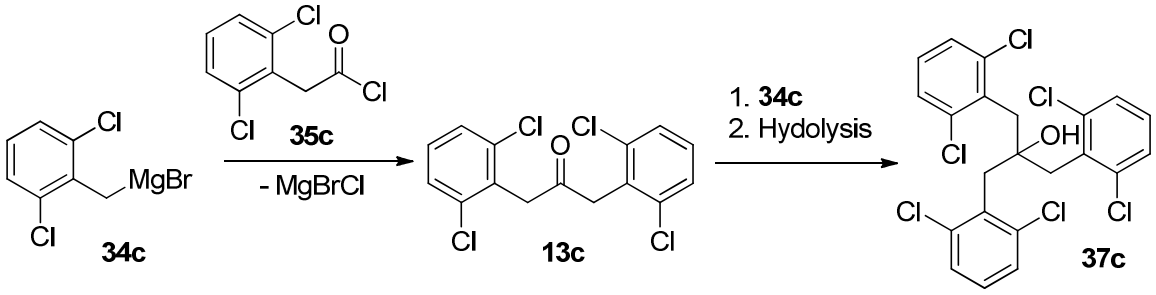

Scheme 46: *Possible side reaction which could occur at room temperature*

Acidic work up and extraction with Et_2O released a yellow solid containing 3 different products as identified by GC-MS analysis. The two major species were the desired ketone **13c** (*348.01amu*) and 1,2-diphenyl ethane **38c** (*320.01 amu*). The latter could be produced during Grignard reagent formation *via* a coupling reaction. Traditionally performed using sodium, this Wurtz reaction would occur according to the mechanism represented in *Scheme 47*. [57]

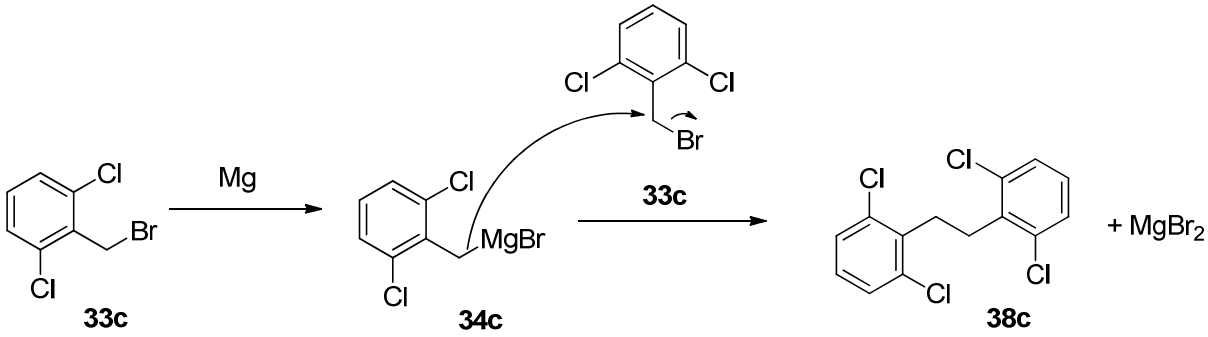

Scheme 47: *Wurtz coupling between **34c** and **33c** giving **38c***

Analysis of the aqueous layer revealed the presence of starting acid **17c**. This was the product of unreacted **35c** hydrolysis during the workup. Due to the little amount of crude solid obtained, no further purification was undertaken.

Conditions known to avoid Wurtz coupling, namely high dilution and the use of magnesium excess were also tested, but unfortunately compound **38c** was still produced.

3 CONCLUSION AND OUTLOOK

The main goal of this Master thesis was unfortunately not reached, as no cyclisation to give the expected buckybowl **16** and thus no formation of complex **16'K** were achieved. Nevertheless, the interest of such molecules for hydrogen storage has been studied *via* DFT calculations. Compared to corannulene, the enhancement of the surface and the complexation of **16'** with alkali ions would give rise to a higher dipole moment. This should stronger polarize hydrogen molecules, thus allowing a possible increase in hydrogen storage capacity. Further investigations could be the creation of a lattice containing molecules of **16'K** at fixed positions modeling a possible solid state. Molecular hydrogen molecules would then be added and molecular dynamics simulation could be run. This procedure, which was achieved by Scanlon et al. for corannulene hydrogen uptake determination [18] , would probably give us an idea of how many hydrogen molecules may be absorbed by such a media.

For the first and second synthetic pathways, problems were unfortunately encountered during the first step, namely the synthesis of bisbenzyl ketones **13b** and **13c**. Dakin-West reaction conditions were found to be unsuccessful while a Claisen condensation only gave poor yields.

A good point of this Master thesis was the postulation of a possible mechanism for the Dakin-West reaction based on ESI^+-MS measurements and DFT calculations. Indeed a possible explanation of the reason why bisbenzyl ketone **13b** and **13c** had never been synthesized using this reaction was postulated thanks to calculations. Once the anhydride formed, DMAP would deprotonate or attack the electrodefficient carbonyl. For *ortho*-dichlorinated **28c**, the nucleophilic product **29c** was preferred by roughly 11 kJ/mol as compared to deprotonated **28'c**. Indeed, the negative charge was less stabilized than in **28'a** due to the presence of donating groups in *ortho*-positions. Another observation was that the carbonyl twisted out of the plane formed by the benzene ring, thus hindering the overlap of p-atomic orbitals of the anion with the π-system of the aromatic. This could be due to electrostatic repulsion between oxygen atoms and the chlorines. This observation was validated by the unsuccessful reaction between DMAP and pre-synthesized **28c**.

Steric hindrance caused by the chlorines toward the base could also be a reason of the reaction failure. This last aspect can be illustrated by Claisen condensation where the yields of bisbenzyl ketone decreased from fluorinated benzyl **13b** to chlorinated benzyl **13c**.

The last approach, namely the synthesis of bisbenzyl ketone **13c** *via* Grignard reaction was not efficient because Wurtz coupling between Grignard reagent **35c** and compound **34c** occurred. This was due to the high reactivity of the benzylic brominated compounds. Starting from 1,3-dichloro-2-(chloromethyl)benzene **38** should be a valuable alternative due to the lower reactivity of chlorinated compared to brominated substituents.

Supposing this alternative would avoid Wurtz coupling, another interesting pathway reported in *Scheme 48* should be tested. This approach would allow the use of **38** as single starting material, forming the Grignard reagent and then transforming one equivalent to the aldehyde *via* a nucleophilic attack on ethyl formate. This would release ethanol and another equivalent of Grignard reagent would form after acidic treatment the coupled alcohol. A Dess-Martin periodinane oxidation should produce the desired bisbenzyl ketone **13c**. Another advantage is that this reaction could be conducted at room temperature as no additional nucleophilic attack could occur on compound **41**.

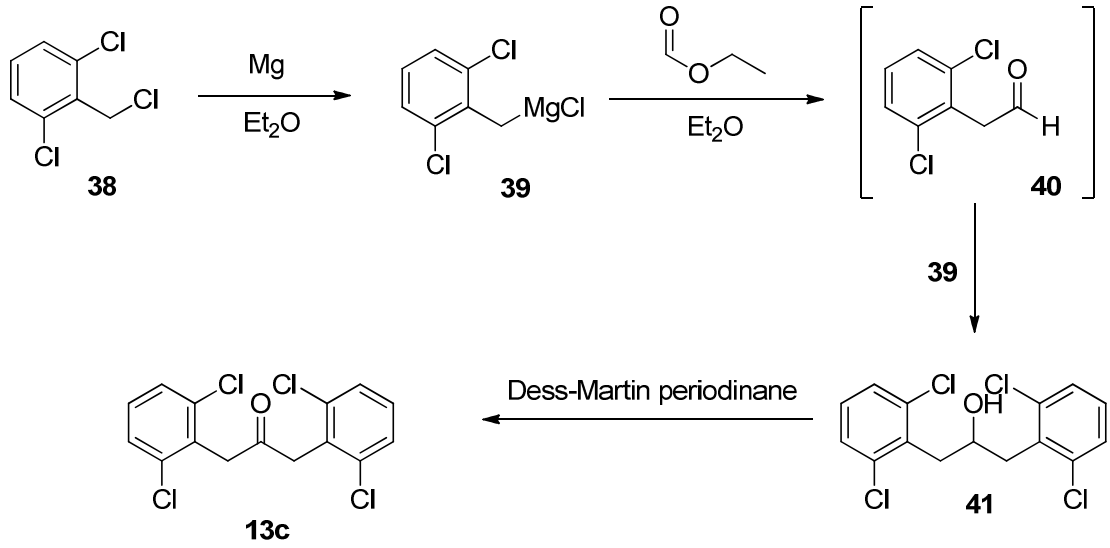

Scheme 48: *New strategy for the synthesis of* ***13c***

Nevertheless the reaction of acyl chloride with Grignard reagent has a main advantage over those represented in *Scheme 48*. Indeed, as represented in *Scheme 49*, it will offers the possibility to synthesize asymmetrical bisbenzyl ketones opening the scope of combining different ring closing techniques.

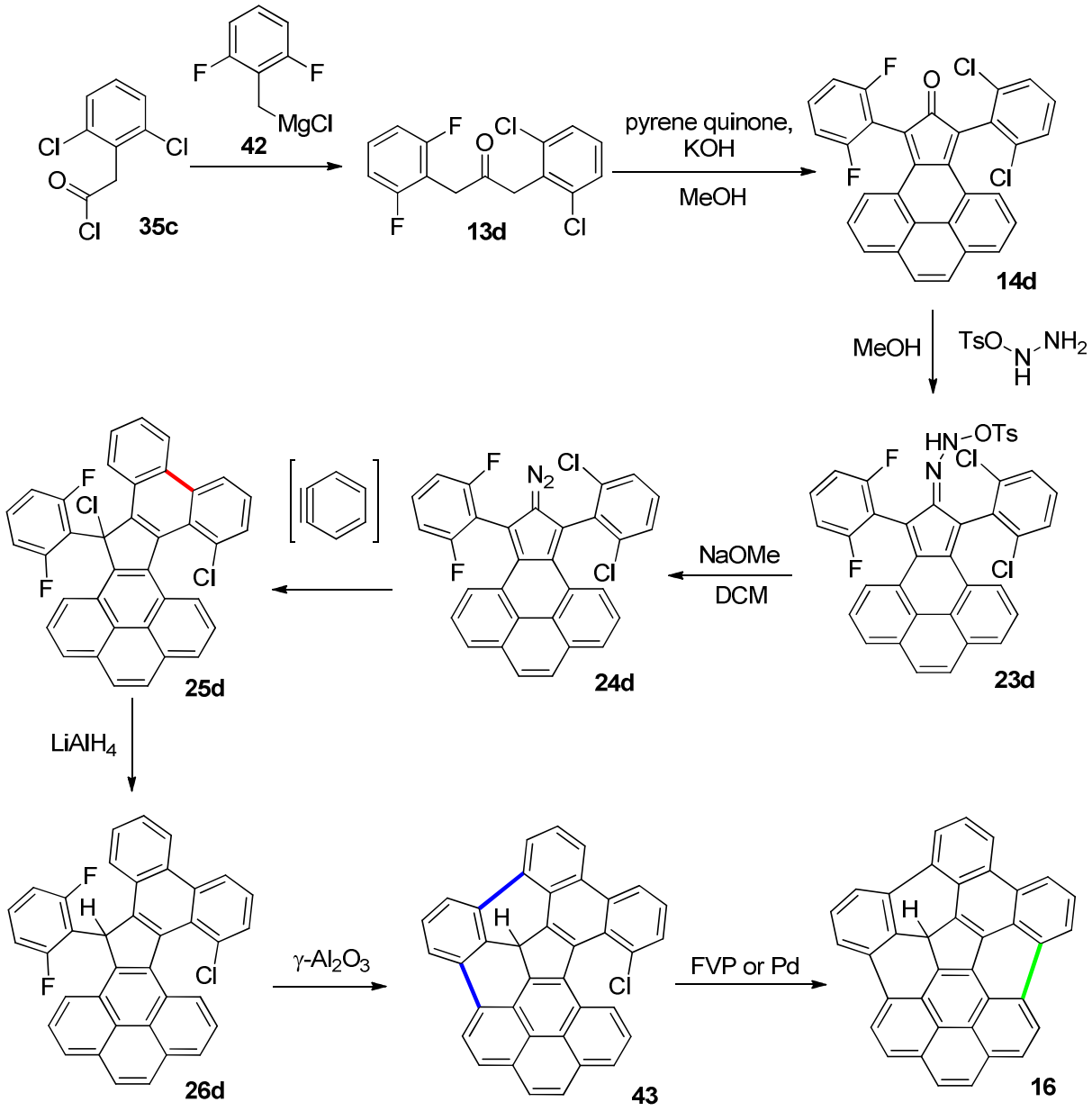

It's believed that HF elimination steps would give compound **43** in nearly quantitative yield since it will not result in high curvature introduction. The last step would be performed *via* FVP or Pd-catalyzed cyclisation which are two methods which have already shown better efficiency in high curvature introduction. [27,28]

4 EXPERIMENTAL PART

4.1 General considerations

All chemicals used in the synthesis were purchased from Sigma-Aldrich, Fluka or Acros and were used without further purification. Technical solvents were distilled prior to use and dry solvents were obtained from a drying system if not indicated otherwise. Other solvents used in reaction mixtures were used as received. The sensitive reactions were conducted under inert atmosphere using dry argon (48) purchased from Carbagas.

Filtrations were achieved over plug of Merck silica gel 60 (0.04-0.063 mm, 230-400 mesh).

IR measurements were performed on a Bruker Tensor 27 equipped with a Golden Gate diamond ATR system. UPLC routine analyzes were performed on a UPLC-MS Waters Acquity equipped with a PDA detector and a simple quad ESI. The column was a BEM C18, 1.7 µm, 2.1 mm x 5 cm. All samples were dissolved in pure MeCN.

NMR spectra were recorded on a Bruker Avance DPX 360 MHz (^{1}H: 360 MHz and ^{13}C: 90 MHz) spectrometer or on a Bruker Avance III 300 MHz (^{1}H: 300 MHz, ^{13}C: 75 MHz, ^{19}F: 300 MHz) using $CDCl_3$ or CD_2Cl_2 as solvents. Chemical shifts are reported in ppm relative to tetramethylsilane (TMS) or to the solvent residual peak. The coupling constants (J) are given in Hz.

4.2 First pathway starting from 2,6-difluorophenylacetic acid

4.2.1 Synthesis of ethyl 2-(2,6-dichlorophenyl)acetate :

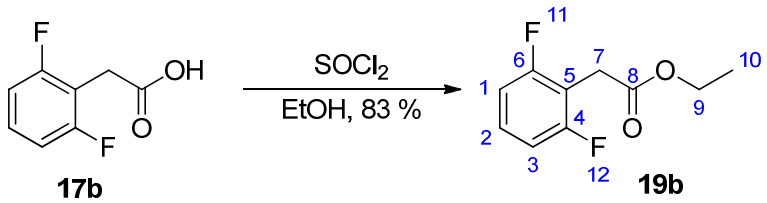

17b 19b

Thionyl chloride (1 ml, 13.77 mmol, 1.1 eq) was added dropwise to a solution of 2-(2,6-difluorophenyl)acetic acid **17b** (2.1 g, 12.20 mmol, 1 eq) in 13 ml of EtOH in an ice-bath. The solution was refluxed for 4 h and concentrated. The residue was diluted with ethyl acetate and washed three times with aqueous 1M NaOH, dried over $MgSO_4$, filtered, and concentrated to dryness to give ethyl 2-(2,6-difluorophenyl)acetate **13b** in 83 % yield (2.027 g, 10.13 mmol) as dark yellow oil. **^{1}H NMR** (300 MHz, CHLOROFORM-*d*) δ ppm 1.25 (t, *J*=7.18 Hz, 3 H, H(10)) 3.70 (s, 2 H, H(9)) 4.18 (q, *J*=7.11 Hz, 2 H, H(7)) 6.76 - 6.98 (m, 2 H, H(1, 3)) 7.11 - 7.36 (m, 1 H, H(2)); **^{13}C NMR** (75 MHz, CHLOROFORM-*d*) δ ppm 13.99 (s, 1 C, C(10)) 27.91 (t, *J*=3.03 Hz, 1 C, C(7)) 61.11 (s, 1 C, C(9)) 110.59 (t, *J*=20.2 Hz, 1 C, C(5)) 110.92 (d, *J*=17.61 Hz, 2 C, C(1, 3)) 128.85 (t, *J*=10.18 Hz, 1 C(2))

161.38 (d, *J*=248.14 Hz, 2 C, C(4, 6)) 169.60 (s, 1 C, C(8)); **^{19}F NMR** (300 MHz, CHLOROFORM-*d*) δ ppm -114.70 (m, 2 F, F(11, 12)) ; **EI-MS** (%) *m/z* 199.88 ($M^{\cdot+}$,16%), 126.83 ($[M\text{-}COOEt]^+$, 100%); **IR** (Golden gate, ATR, cm^{-1}) 1743 (s), 1630 (w), 1595 (w), 1471 (s), 1240 (w), 1216 (w), 1173 (w), 1019 (m), 785 (w), 630.73 (s).

4.2.2 Synthesis of 1,3-bis(2,6-difluorophenyl)propan-2-one:

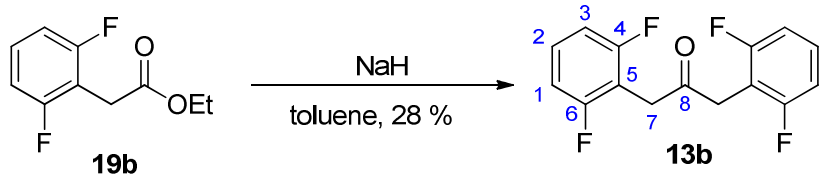

To a suspension of NaH (60 wt% in mineral oil, 69.2mg, 1.731 mmol, 0.66 eq) in dry toluene (1 ml) was added dropwise to a solution of ethyl 2-(2,6-fluorophenyl)acetate **19b** (525 mg, 2.62 mmol, 1 eq) in dry toluene (1 ml). The reaction mixture was heated to 75°C for 1.5 h and then cooled to 0°C and quenched with 1 ml of cold HCl (7.6 M). The solvent was removed and 1 ml of AcOH (96 %) and 1.5 ml of HCl (20 %) were added to the remaining residue. Then reaction mixture was heated to reflux overnight. The resulting solution was diluted with 20 ml of water and extracted twice with 50 ml of DCM. The organic layers were combined and washed twice with 25 ml of NaOH (1M), dried over $MgSO_4$, filtered and concentrated to dryness to give a yellowish mixture which was recrystallized in 4 ml of heptane offering 1,3-bis(2,6-difluorophenyl)propan-2-one **13b** in 28 % yield (102 mg, 0.361 mmol) as white needles. **^{1}H NMR** (300 MHz, DICHLOROMETHANE-d_2) δ ppm 3.91 (s, 4 H, H(7)) 6.83 - 7.02 (m, 4 H, H(1, 3)) 7.17 - 7.39 (m, 2 H, H(2)); **^{13}C NMR** (75 MHz, DICHLOROMETHANE-d_2) δ ppm 36.37 (s, 2 C, C(7)) 110.10 - 112.36 (m, 6 C, C(1, 2, 3)) 129.71 (t, *J*=10.18 Hz, 2 C, C(5, 10)) 161.92 (d, *J*=247.59 Hz, 4 C, C(4, 6)) 200.74 (s, 1 C, C(8)); **ESI-MS**: *m/z* 282.13 $[M + H]^+$, 324.17 $[M + H + MeCN]^+$; **IR** (Golden gate, ATR, cm^{-1}) 1717 (w), 1629 (w), 1594 (m), 1470 (s), 1402 (w), 1337 (w), 1269 (m), 1218 (m), 1062 (m), 1029 (s), 883 (w), 785 (s), 754 (w), 687 (m).

4.3 Second Pathway

4.3.1 Synthesis of 1,3-diphenylpropan-2-one:

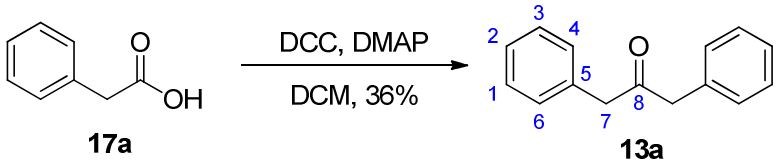

A solution of DCC (758 mg, 3.67 mmol, 1 eq) and DMAP (112 mg, 0.918 mmol, 0.25 eq) in DCM (4 mL) was stirred at 25 °C under dry Ar and treated dropwise with a solution of phenylacetic acid **17a**

(500 mg, 3.67 mmol, 1 eq) in DCM (4 mL). The resulting mixture was stirred at 25 °C for 24 h and the precipitated solid was removed by filtration over a plug of silica gel (eluent: DCM/pentane 9:1). The solvent was removed and the obtained yellow oil was recrystallized from ethanol in the freezer to give 1,3-diphenylpropan-2-one **13a** as a light yellowish solid (oil at r.t.) in 36 % yield (139 mg, 0.661 mmol).**^{1}H NMR** (360 MHz, CHLOFORM-*d*) δ ppm 3.72 (s, 4H, H(7)), 7.15 (d, *J* = 6.81 Hz, 4H, H(4, 6)), 7.21 – 7.39 (m, 6H, H(1, 2, 3)) ; **^{13}C NMR** (91 MHz, CHLOROFORM-*d*) δ ppm 49.06 (s, 2C, C(7), 127.04 (s, 2C, C(2)), 128.70 (s, 4C, C(1, 3)), 129.47 (s, 4C, C(4, 6)), 133.94 (s, 2C, C(5)), 205.68 (s, 1C, C(8)) ; **ESI-MS**: *m/z* 211.18 $[M + H]^+$; **IR** (Golden gate, ATR, cm^{-1}) 1708 (s), 1493 (m), 1453 (w), 1337 (w), 1168 (w), 1092 (w), 1061 (w), 1030 (w), 750 (m), 725 (m), 692 (s), 637 (m).

4.3.2 Synthesis of 2-phenylacetic anhydride:

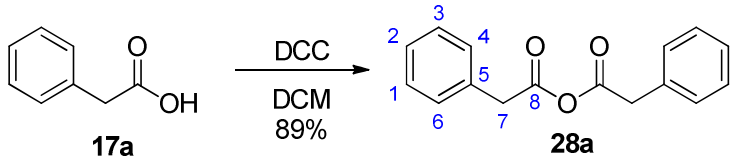

A solution of DCC (206 mg, 1 mmol, 0.5 eq) in dry DCM (7 ml) was added to a solution of 2-phenylacetic acid **17a** (272 mg, 2 mmol, 1 eq) in dry DCM (10 ml). The reaction mixture was kept at room temperature overnight. The white precipitate was removed by filtration and the solvent was removed by evaporation under reduced pressure. The solid was dissolved in acetonitrile and the obtained white suspension was filtered. The mixture was concentrated to dryness offering 2-phenylacetic anhydride **28a** in 89 % yield (227 mg, 0.893 mmol) as a white solid. **^{1}H NMR** (300 MHz, DICHLOROMETHANE-d_2) δ ppm 3.74 (s, 4 H, H(7)) 7.23 (m, 4H, H(4, 6)), 7.33 (m, 6H, H(1, 2, 3)); **^{13}C NMR** (75 MHz, DICHLOROMETHANE-d_2) δ ppm 42.44 (s, 2 C, C(7)) 128.09 (s, 2 C, C(2)) 129.25 (s, 4 C, C(1, 3)) 130.01 (s, 4 C, C(4, 6)) 132.85 (s, 2 C, C(5)), 167.65 (s, 2C, C(8)) ; **ESI-MS**: *m/z* 277.09 $[M + Na]^+$, 318.13 $[M+ Na + MeCN]^+$; **IR** (Golden gate, ATR, cm^{-1}) 1811 (s), 1693 (s), 1498 (w), 1407 (m), 1336 (w), 1226 (m), 1187 (w), 1029 (w), 902 (m), 839 (w), 751 (m), 698 (s), 676 (m).

4.3.3 Synthesis of 2-(2,6-dichlorophenyl)acetic anhydride:

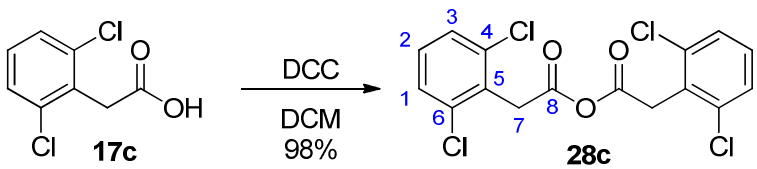

A solution of DCC (201 mg, 0.975 mmol, 0.5 eq) in dry DCM (7 ml) was added to a solution of 2-(2,6-dichlorophenyl)acetic acid **17c** (400 mg, 1.951 mmol, 1 eq) in dry DCM (10 ml). The reaction mixture was kept at room temperature overnight. The DCU precipitate was removed by filtration and

the solvent was removed by evaporation under reduced pressure. The solid was dissolved in acetonitrile and the obtained suspension was filtered. The mixture was concentrated to dryness offering 2-(2,6-dichlorophenyl)acetic acid **28c** in 98 % yield (375 mg, 0.956 mmol) as a white solid. **^{1}H NMR** (300 MHz, CHLOROFORM-*d*) δ ppm 4.16 (s, 4 H, H(7)) 7.18 – 7.22 (m, 2 H, H(2), 7.31 – 7.34 (m, 4H, H(1, 3); **^{13}C NMR** (75 MHz, DICHLOROMETHANE-d_2) δ ppm 37.61 (s, 2C, C(7)), 128.13 (s, 6C, C(1, 3, 5)), 129.47 (s, 2C, C(2)), 136.11 (s, 4C, C(4, 6)), 164.36 (s, 2C, C(8)) ; **ESI-MS**: *m/z* 413.03 $[C_{16}H_{10}{}^{35}Cl_4O_3 + Na]^+$, 414.98 $[C_{16}H_{10}{}^{35}Cl_3{}^{37}ClO_3 + Na]^+$, 454.02 $[C_{16}H_{10}{}^{35}Cl_4O_3 + Na + MeCN]^+$, 455.97 $[C_{16}H_{10}{}^{35}Cl_3{}^{37}ClO_3 + Na + MeCN]^+$; **IR** (Golden gate, ATR, cm^{-1}) 1810 (m), 1745 (m), 1563 (w), 1436 (m), 1328 (w), 1207 (w), 1094 (s), 1047 (s), 929 (m), 897 (m), 781 (m), 764 (s), 689 (w), 672 (m).

4.3.4 Synthesis of 1,3-diphenylpropan-2-one:

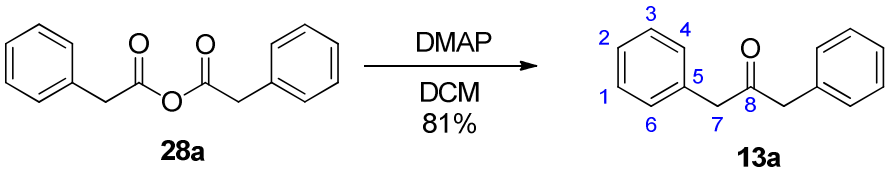

28a **13a**

A solution of DMAP (42 mg, 0.344 mmol, 0.25 eq) in dry DCM (3 ml) was added to **28a** (350 mg, 1.376 mmol, 1 eq) in dry DCM (3 ml) and the reaction was stirred during 2 hours. 25 ml of HCl (1 M) were added and the organic layer was separated and washed with $NaHCO_3$ (conc.). Evaporation of DCM afforded 1,3-diphenylpropan-2-one **13a** in 81% yield (235 mg, 1.118 mmol) as yellowish oil which crystalized in the fridge. **^{1}H NMR** (360 MHz, CHLOFORM-*d*) δ ppm 3.72 (s, 4H, H(7)), 7.15 (d, *J* = 6.81 Hz, 4H, H(4, 6)), 7.20 – 7.39 (m, 6H, H(1, 2, 3)) ; **^{13}C NMR** (91 MHz, CHLOROFORM-*d*) δ ppm 49.05 (s, 2C, C(7), 127.04 (s, 2C, C(2)), 128.71 (s, 4C, C(1, 3)), 129.47 (s, 4C, C(4, 6)), 133.95 (s, 2C, C(5)), 205.68 (s, 1C, C(8)) ; **ESI-MS**: *m/z* 211.18 $[M + H]^+$; **IR** (Golden gate, ATR, cm^{-1}) 1710 (s), 1490 (m), 1455 (w), 1335 (w), 1168 (w), 1093 (w), 1062 (w), 1031 (w), 750 (m), 726 (m), 693 (s), 637 (m).

4.3.5 Synthesis of ethyl 2-(2,6-dichlorophenyl)acetate :

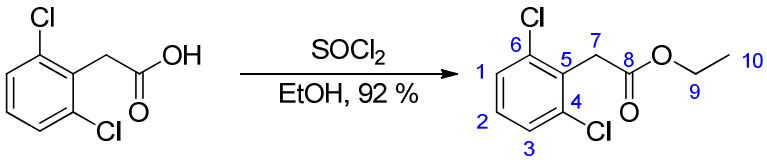

17c **19c**

Thionyl chloride (1.2 ml, 16.52 mmol, 1.1 eq) was added dropwise to a solution of 2-(2,6-dichlorophenyl)acetic acid **19c** (2.997 g, 14.62 mmol, 1 eq) in 15 ml of EtOH in an ice-bath. The solution was refluxed for 4 h and concentrated. The residue was diluted with ethyl acetate and washed three times with aqueous 1M NaOH, dried over $MgSO_4$, filtered, and concentrated to dryness to give

ethyl 2-(2,6-dichlorophenyl)acetate **13c** in 92 % yield (3.136 g, 13.45 mmol) as white solid; **^{1}H NMR** (300 MHz, CHLOROFORM-*d*) δ ppm 1.24 (t, *J*=7.08 Hz, 3 H, H(10)) 3.99 (s, 2 H, H(9)) 4.17 (q, *J*=7.11 Hz, 2 H, H(7)) 7.01 - 7.19 (m, 1 H, H(2)) 7.28 (d, *J*=8.12 Hz, 2 H, H(1,3)); **^{13}C NMR** (75 MHz, CHLOROFORM-*d*) δ ppm 13.93 (s, 1C, C(10)) 36.53 (s, 1 C, C(7)) 60.90 (s,1 C, C(9)) 127.79 (s, 2 C, C(1, 3)) 128.67 (s, 1 C, C(2)) 131.12 (s, 1 C, C(5)) 135.87 (s, 2 C, C(4, 6)) 169.11 (s, 1 C, C(8)); **EI-MS** (%) *m/z* 232.98 ($M^{\cdot+}$,5.4%), 196.85 ($[M\text{-}Cl]^{+}$,45%), 158.77, ($[M\text{-}2Cl]^{\cdot+}$,100%); **IR** (Golden gate, ATR, cm^{-1}) 1736 (m), 1626 (m-s), 1589 (m-s), 1311 (m), 1216 (m-s), 1019 (s), 976 (s), 935 (m-s), 915 (m-s).

4.3.6 Synthesis of 1,3-bis(2,6-dichlorophenyl)propan-2-one:

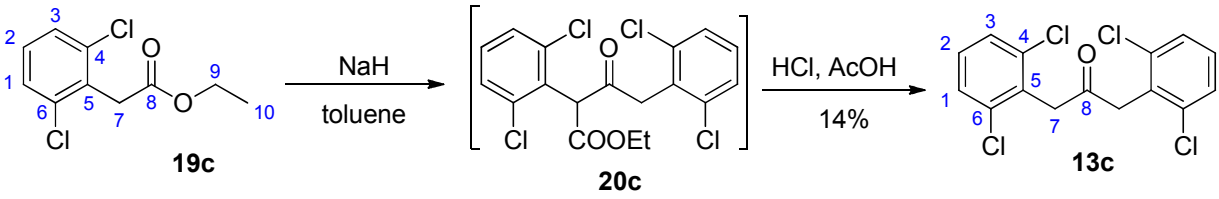

To a suspension of NaH (60 wt% in mineral oil, 63.1 mg, 1.577 mmol, 0.66 eq) in dry toluene (0.5 ml) was added dropwise a solution of ethyl 2-(2,6-dichlorophenyl)acetate **19c** (557 mg, 2.39 mmol, 1 eq) in dry toluene (0.5 ml). The reaction mixture was heated to 75°C for 1.5 h and then cooled to 0°C and quenched with 1 ml of cold HCl (7.6 M). The solvent was then removed. To the remaining residue, 1 ml of AcOH (96 %) and 1.5 ml of HCl (20 %) were added and the reaction mixture was heated to reflux overnight. The resulting solution was diluted with 20 ml of water and extracted twice with 25 ml of DCM. The organic layer were combined and washed twice with 25 ml of NaOH (1M), dried over $MgSO_4$, filtered and concentrated to dryness to give a yellowish mixture which was recrystallized in 4 ml heptane offering 1,3-bis(2,6-dichlorophenyl)propan-2-one **13c** in 14 % (59 mg, 0.17 mmol) as a dark yellow solid. **^{1}H NMR** (300 MHz, DICHLOROMETHANE-d_2) δ ppm 4.22 (s, 4 H, H(7, 9)) 7.16 - 7.25 (m, 2 H, H(2)) 7.33 - 7.39 (m, 4 H, H(1, 3)); **^{13}C NMR** (75 MHz, DICHLOROMETHANE-d_2) δ ppm 45.27 (s, 2 C, C(7)) 128.46 (s, 4 C, C(1, 3)) 129.47 (s, 2 C, C(2)) 131.98 (s, 2 C, C(5)) 136.44 (s, 4 C, C(4, 6)) 200.31 (s, 1 C, C(8)); **ESI-MS**: *m/z* 347.05 $[C_{15}H_{10}{}^{35}Cl_4O + H]^+$, 349.08 $[C_{15}H_{10}{}^{35}Cl_3{}^{37}ClO + H]^+$, 351.02 $[C_{15}H_{10}{}^{35}Cl_2{}^{37}Cl_2O + H]^+$, 388.08 $[C_{15}H_{10}{}^{35}Cl_4O + H + MeCN]^+$, 390.05 $[C_{15}H_{10}{}^{35}Cl_3{}^{37}ClO + H + MeCN]^+$, 392.04 $[C_{15}H_{10}{}^{35}Cl_2{}^{37}Cl_2O + H + MeCN]^+$; **IR** (Golden gate, ATR, cm^{-1}) 1713 (m), 1564 (w), 1435 (s), 1330 (m), 1178 (w), 1152 (w), 1088 (m), 1059 (m), 948 (m), 778 (s), 763 (s), 706 (w), 659 (m).

4.3.7 Synthesis of 2-(2,6-dichlorophenyl)acetyl chloride:

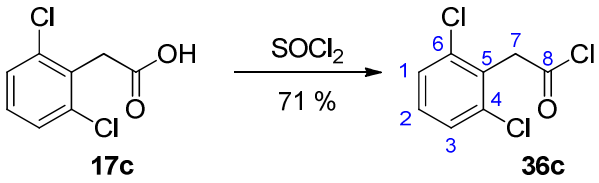

2-(2,6-dichlorophenyl)acetic acid **17c** (2 g, 9.75 mmol, 1 eq) in 2,4 ml of thionyl chloride (32.9 mmol, 3.37 eq) was stirred at 65°C. After 2 hours, the solution was concentrated to give orange liquid. Distillation under 0.5 mbar and 125°C give the desired 2-(2,6-dichlorophenyl)acetyl chloride **36c** in 71 % (1.55 g, 6.94 mmol) as a colorless oil. **^{1}H NMR** (360 MHz, CHLOFORM-*d*) δ ppm 4.54 (s, 2H, H(7)), 7.19 – 7.28 (m, 1H, H(2)), 7.32 – 7.41 (m, 2H, H(1, 3)); **^{13}C NMR** (91 MHz, CHLOROFORM-*d*) δ ppm 46.91 (s, 1C, C(7)), 127.01 (s, 2C, C(1, 3)), 128.00 (s, 1C, C(5)), 128.84 (s, 1C, C(2)), 134.82 (s, 2C, C(4, 6), 168.69 (s, 1C, C(8)); **ESI-MS**: *m/z* 246.11 $[C_8H_5{}^{35}Cl_3O + Na]^+$, 248.10 $[C_8H_5{}^{35}Cl^{37}ClO_3 + Na]^+$; **IR** (Golden gate, ATR, cm^{-1}) 1792 (s), 1583 (w), 1565 (m), 1437 (s), 1403 (m), 1316 (w), 1170 (w), 1091 (m), 961 (s), 910 (m), 763 (s), 684 (s), 609 (s).

5 REFERENCES

(1) Barbir, F. *PEM Fuel Cells: Theory and Practice*; Academic Press, **2012**.

(2) HowStuffWorks "How Fuel Cells Work", http://auto.howstuffworks.com/fuel-efficiency/alternative-fuels/fuel-cell.htm.

(3) Fuel Cell Market (Global) by Technology, Application, Component, Installation, Cost, Geography, Trends and Forecasts (2011 – 2016), Fuel Cell Market Research Report :Marketsandmarkets, http://www.marketsandmarkets.com/Market-Reports/fuel-cell-market-348.html

(4) Shaw, L.; Pratt, J.; Klebanoff, L.; Johnson, T.; Arienti, M.; Moreno, M. Analysis of H2 storage needs for early market "man-portable" fuel cell applications. *International Journal of Hydrogen Energy* **2013**, *38*, 2810–2823.

(5) Schlapbach, L.; Züttel, A. Hydrogen-storage materials for mobile applications. *Nature* **2001**, *414*, 353–358.

(6) Energy Content of Selected Fuels, http://arewetoast.com/energy-content-of-selected-fuels.html

(7) U.S. Department of Energy, Fuel cell technologies program, **2011**.

(8) Ross, D. K. Hydrogen storage: The major technological barrier to the development of hydrogen fuel cell cars. *Vacuum* **2006**, *80*, 1084–1089.

(9) BMW EfficientDynamics : BMW CleanEnergy http://www.bmw.com/com/en/insights/technology/efficient_dynamics/phase_2/clean_energy/bmw_hydrogen_7.html

(10) Graetz, J. Metastable Metal Hydrides for Hydrogen Storage. *ISRN Materials Science* **2012**, *2012*, 1–18.

(11) Duksh, Y. S.; Kaushik, B. K.; Sarkar, S.; Singh, R. Performance comparison of carbon nanotube, nickel silicide nanowire and copper VLSI interconnects: Perspectives and challenges ahead. *Journal of Engineering, Design and Technology* **2010**, *8*, 334–353.

(12) Zhu, Y. A.; Sui, Z. J.; Zhao, T. J.; Dai, Y. C.; Cheng, Z. M.; Yuan, W. K. Modeling of fishbone-type carbon nanofibers: A theoretical study. *Carbon* **2005**, *43*, 1694–1699.

(13) Evans, A.; van Loon, J. T.; Woodward, C. E.; Gehrz, R. D.; Clayton, G. C.; Helton, L. A.; Rushton, M. T.; Eyres, S. P. S.; Krautter, J.; Starrfield, S.; Wagner, R. M. Solid-phase C60 in the peculiar binary XX Oph? *Monthly Notices of the Royal Astronomical Society: Letters* **2012**, *421*, L92–L96.

(14) Banerjee, S.; Murad, S.; Puri, I. K. Hydrogen Storage in Carbon Nanostructures: Possibilities and Challenges for Fundamental Molecular Simulations. *Proceedings of the IEEE* **2006**, *94*, 1806–1814.

(15) Denis, P. A. Investigation of H2 Physisorption on Corannulene (C20H10), Tetraindenocorannulene (C44H18), Pentaindenocorannulene (C50H20), C60, and Their Nitrogen Derivatives. *J. Phys. Chem. C* **2008**, *112*, 2791–2796.

(16) Scott, L. T.; Bronstein, H. E.; Preda, D. V.; Ansems, R. B. M.; Bratcher, M. S.; Hagen, S. Geodesic polyarenes with exposed concave surfaces. *Pure and Applied Chemistry* **1999**, *71*, 209–219.

(17) Scanlon, L. G.; Feld, W. A.; Balbuena, P. B.; Sandi, G.; Duan, X.; Underwood, K. A.; Hunter, N.; Mack, J.; Rottmayer, M. A.; Tsao, M. Hydrogen Storage Based on Physisorption. *J. Phys. Chem. B* **2009**, *113*, 4708–4717.

(18) Scanlon, L. G.; Balbuena, P. B.; Zhang, Y.; Sandi, G.; Back, C. K.; Feld, W. A.; Mack, J.; Rottmayer, M. A.; Riepenhoff, J. L. Investigation of Corannulene for Molecular Hydrogen Storage via Computational Chemistry and Experimentation. *J. Phys. Chem. B* **2006**, *110*, 7688–7694.

(19) Chen, P.; Wu, X.; Lin, J.; Tan, K. L. High H2 Uptake by Alkali-Doped Carbon Nanotubes Under Ambient Pressure and Moderate Temperatures. *Science* **1999**, *285*, 91–93.

(20) Banerjee, S.; Pillai, C. G. S.; Majumder, C. Hydrogen absorption behavior of doped corannulene: A first principles study. *International Journal of Hydrogen Energy* **2011**, *36*, 4976–4983.

(21) Simonyan, V. V.; Diep, P.; Johnson, J. K. Molecular simulation of hydrogen adsorption in charged single-walled carbon nanotubes. *The Journal of Chemical Physics* **1999**, *111*, 9778–9783.

(22) Zabula, A. V.; Spisak, S. N.; Filatov, A. S.; Grigoryants, V. M.; Petrukhina, M. A. How Charging Corannulene with One and Two Electrons Affects Its Geometry and Aggregation with Sodium and Potassium Cations. *Chemistry – A European Journal* **2012**, *18*, 6476–6484.

(23) Scott, L. T.; Cheng, P.-C.; Hashemi, M. M.; Bratcher, M. S.; Meyer, D. T.; Warren, H. B. Corannulene. A Three-Step Synthesis1. *J. Am. Chem. Soc.* **1997**, *119*, 10963–10968.

(24) Bronstein, H. E.; Choi, N.; Scott, L. T. Practical Synthesis of an Open Geodesic Polyarene with a Fullerene-type 6:6-Double Bond at the Center: Diindeno[1,2,3,4-defg;1‘,2‘,3‘,4‘-mnop]chrysene. *J. Am. Chem. Soc.* **2002**, *124*, 8870–8875.

(25) Butterfield, A. M.; Gilomen, B.; Siegel, J. S. Kilogram-Scale Production of Corannulene. *Org. Process Res. Dev.* **2012**, *16*, 664–676.

(26) Scott, L. T.; Jackson, E. A.; Zhang, Q.; Steinberg, B. D.; Bancu, M.; Li, B. A Short, Rigid, Structurally Pure Carbon Nanotube by Stepwise Chemical Synthesis. *J. Am. Chem. Soc.* **2012**, *134*, 107–110.

(27) Mizyed, S.; Georghiou, P. E.; Bancu, M.; Cuadra, B.; Rai, A. K.; Cheng, P.; Scott, L. T. Embracing C60 with Multiarmed Geodesic Partners. *J. Am. Chem. Soc.* **2001**, *123*, 12770–12774.

(28) Jackson, E. A.; Steinberg, B. D.; Bancu, M.; Wakamiya, A.; Scott, L. T. Pentaindenocorannulene and Tetraindenocorannulene: New Aromatic Hydrocarbon π Systems with Curvatures Surpassing That of C60. *J. Am. Chem. Soc.* **2007**, *129*, 484–485.

(29) Wang, L.; Shevlin, P. B. Palladium-Mediated Formation of Bowl-Shaped PAHs: Synthesis of as-Indaceno[3,2,1,8,7,6,-pqrstuv]picenes. *Org. Lett.* **2000**, *2*, 3703–3705.

(30) Amsharov, K. Y.; Kabdulov, M. A.; Jansen, M. Facile Bucky-Bowl Synthesis by Regiospecific Cove-Region Closure by HF Elimination. *Angewandte Chemie International Edition* **2012**, *51*, 4594–4597.

(31) Amsharov, K. Y.; Merz, P. Intramolecular Aryl–Aryl Coupling of Fluoroarenes through Al2O3-Mediated HF Elimination. *J. Org. Chem.* **2012**, *77*, 5445–5448.

(32) Thilgen, C. Synthesis of Geodesic Polynuclear Arenes and Fullerenes by Intramolecular Aryl–Aryl Coupling. *Angewandte Chemie International Edition* **2012**, *51*, 7082–7084.

(33) Fragnière, N. New polycondensed aromatic compounds for applications in the hydrogen cycle, Université de Fribourg : Fribourg, **2011**

(34) Weber, P. Synthesis towards bowl-shaped molecules based on corannulene, aiming hydrogen storage, Université de Fribourg : Fribourg, **2012**

(35) Lee, C.; Yang, W.; Parr, R. G. Development of the Colle-Salvetti correlation-energy formula into a functional of the electron density. *Phys. Rev. B* **1988**, *37*, 785–789.

(36) Gaussian 09, Revision C.01, M. J. Frisch, G. W. Trucks, H. B. Schlegel, G. E. Scuseria, M. A. Robb, J. R. Cheeseman, G. Scalmani, V. Barone, B. Mennucci, G. A. Petersson, H. Nakatsuji, M. Caricato, X. Li, H. P. Hratchian, A. F. Izmaylov, J. Bloino, G. Zheng, J. L. Sonnenberg, M. Hada, M. Ehara, K. Toyota, R. Fukuda, J. Hasegawa, M. Ishida, T. Nakajima, Y. Honda, O. Kitao, H. Nakai, T. Vreven, J. A. Montgomery, Jr., J. E. Peralta, F. Ogliaro, M. Bearpark, J. J. Heyd, E. Brothers, K. N. Kudin, V. N. Staroverov, R. Kobayashi, J. Normand, K. Raghavachari, A. Rendell, J. C. Burant, S. S. Iyengar, J. Tomasi, M. Cossi, N. Rega, J. M. Millam, M. Klene, J. E. Knox, J. B. Cross, V. Bakken, C. Adamo, J. Jaramillo, R. Gomperts, R. E. Stratmann, O. Yazyev, A. J. Austin, R. Cammi, C. Pomelli, J. W. Ochterski, R. L. Martin, K. Morokuma, V. G. Zakrzewski, G. A. Voth, P. Salvador, J. J. Dannenberg, S. Dapprich, A. D. Daniels, Ö. Farkas, J. B. Foresman, J. V. Ortiz, J. Cioslowski, and D. J. Fox, Gaussian, Inc., Wallingford CT, **2009**.

(37) Spartan'10, Wavefunction, Inc. Irvine, CA

(38) Martinez, C. R.; Iverson, B. L. Rethinking the term "pi-stacking."*Chem. Sci.* **2012**, *3*, 2191–2201.

(39) Amsharov, K. Y.; Kabdulov, M. A.; Jansen, M. Homo-elimination of HF—An Efficient Approach for Intramolecular Aryl–Aryl Coupling. *Chemistry – A European Journal* **2010**, *16*, 5868–5871.

(40) Bhandari, S.; Ray, S. A Novel Synthesis of Bisbenzyl Ketones by DCC Induced Condensation of Phenylacetic Acid. *Synthetic Communications* **1998**, *28*, 765–771.

(41) Sauriat-Dorizon, H.; Maris, T.; Wuest, J. D.; Enright, G. D. Molecular Tectonics. Construction of Porous Hydrogen-Bonded Networks from Bisketals of Pentaerythritol. *J. Org. Chem.* **2003**, *68*, 240–246.

(42) Verho, O.; Johnston, E. V.; Karlsson, E.; Bäckvall, J.-E. Tuning of the Electronic Properties of a Cyclopentadienylruthenium Catalyst to Match Racemization of Electron-Rich and Electron-Deficient Alcohols. *Chemistry – A European Journal* **2011**, *17*, 11216–11222.

(43) Renz, M.; Corma, A. Ketonic Decarboxylation Catalysed by Weak Bases and Its Application to an Optically Pure Substrate. *European Journal of Organic Chemistry* **2004**, *2004*, 2036–2039.

(44) Renz, M. Ketonization of Carboxylic Acids by Decarboxylation: Mechanism and Scope. *European Journal of Organic Chemistry* **2005**, *2005*, 979–988.

(45) Fluorinated Building Blocks, http://www.sigmaaldrich.com/chemistry/chemistry-products.html?TablePage=111283772.

(46) Romer, D. Convenient Laboratory Method for the Synthesis of Symmetrical 1,3-Diphenylacetone Derivatives. *Synthesis* **2011**, *2011*, 2721–2723.

(47) Preparation of ethyl esters from carboxylic acids and ethanol using thionyl chloride, http://syntheticfocus.com/esters-2/preparation-of-esters-from-carboxylic-acids/preparation-of-ethyl-esters-from-carboxylic-acids-and-ethanol-using-thionyl-chloride/.

(48) Ho, T.-L.; Jou, D.-G. Synthesis of Cryptolepine and Cryptoteckieine from a Common Intermediate. *Helvetica Chimica Acta* **2002**, *85*, 3823–3827.

(49) Resendiz, M. J. E.; Garcia-Garibay, M. A. Hammett Analysis of Photodecarbonylation in Crystalline 1,3-Diarylacetones. *Org. Lett.* **2005**, *7*, 371–374.

(50) Dalla-Vechia, L.; Santos, V. G.; Godoi, M. N.; Cantillo, D.; Kappe, C. O.; Eberlin, M. N.; Souza, R. O. M. A. de; Miranda, L. S. M. On the mechanism of the Dakin–West reaction. *Org. Biomol. Chem.* **2012**.

(51) Miertuš, S.; Scrocco, E.; Tomasi, J. Electrostatic interaction of a solute with a continuum. A direct utilizaion of AB initio molecular potentials for the prevision of solvent effects. *Chemical Physics* **1981**, *55*, 117–129.

(52) Tran, K.-V.; Bickar, D. Dakin−West Synthesis of β-Aryl Ketones. *J. Org. Chem.* **2006**, *71*, 6640–6643.

(53) Selinger, Z.; Lapidot, Y. Synthesis of fatty acid anhydrides by reaction with dicyclohexylcarbodiimide. *J. Lipid Res.* **1966**, *7*, 174–175.

(54) Goodman, Murray; Toniolo, Claudio; Moroder, Luis; Felix, Aurthur. Houben-Weyl Methods in Organic Chemistry, Volume E22, Synthesis of Peptides and Peptidomimetics, Volumes 1-5 (Workbench Edition), **2004**.

(55) Takahashi, K.; Kobayashi, A.; Doi, M.; Adachi, S.; Taguchi, T.; Okamura, T.; Yamamoto, H.; Ueyama, N. Restriction of CaCO3 polymorph by NHO hydrogen-bonded poly(methacryloylaminocarboxylate) ligands: induced polymorph change by strength and/or formation manner of hydrogen bond. *J. Mater. Chem.* **2005**, *15*, 2178–2187.

(56) Turro, N. J.; Weed, G. C. Micellar systems as supercages for reactions of geminate radical pairs. Magnetic effects. *J. Am. Chem. Soc.* **1983**, *105*, 1861–1868.

(57) Wurtz, A. Ueber eine neue Klasse organischer Radicale. *Annalen der Chemie und Pharmacie* **1855**, *96*, 364–375.